creative commons

COMMONS DEED

저작자표시-비영리-변경금지 2.0 대한민국

이용자는 아래의 조건을 따르는 경우에 한하여 자유롭게

- 이 저작물을 복제, 배포, 전송, 전시, 공연 및 방송할 수 있습니다.

다음과 같은 조건을 따라야 합니다:

저작자표시. 귀하는 원저작자를 표시하여야 합니다.

비영리. 귀하는 이 저작물을 영리 목적으로 이용할 수 없습니다.

변경금지. 귀하는 이 저작물을 개작, 변형 또는 가공할 수 없습니다.

- 귀하는, 이 저작물의 재이용이나 배포의 경우, 이 저작물에 적용된 이용허락조건을 명확하게 나타내어야 합니다.
- 저작권자로부터 별도의 허가를 받으면 이러한 조건들은 적용되지 않습니다.

저작권법에 따른 이용자의 권리는 위의 내용에 의하여 영향을 받지 않습니다.

이것은 이용허락규약(Legal Code)을 이해하기 쉽게 요약한 것입니다.

Disclaimer

dCollection

ULSAN NATIONAL INSTITUTE OF
SCIENCE AND TECHNOLOGY

Master's Thesis

Development of Novel Chemical Tools towards Single or Multiple Pathogenic Elements in Alzheimer's Disease

Jiyeon Han

Department of Chemistry

Graduate School of UNIST

2018

ULSAN NATIONAL INSTITUTE OF
SCIENCE AND TECHNOLOGY

Development of Novel Chemical Tools towards Single or Multiple Pathogenic Elements in Alzheimer's Disease

Jiyeon Han

Department of Chemistry

Graduate School of UNIST

ULSAN NATIONAL INSTITUTE OF SCIENCE AND TECHNOLOGY

Development of Novel Chemical Tools towards Single or Multiple Pathogenic Elements in Alzheimer's Disease

A thesis submitted to the Graduate School of UNIST
in partial fulfillment of the requirements
for the degree of Master of Science

Jiyeon Han

12. 06. 2017

Approved by

Advisor
Associate Professor Mi Hee Lim

ULSAN NATIONAL INSTITUTE OF
SCIENCE AND TECHNOLOGY

Development of Novel Chemical Tools towards Single or Multiple Pathogenic Elements in Alzheimer's Disease

Jiyeon Han

This certifies that the thesis of Jiyeon Han is approved.

12. 06. 2017

Signature

Advisor: Associate Professor Mi Hee Lim

Signature

Assistant Professor Tae-Hyuk Kwon

Signature

Assistant Professor Jung-Min Kee

ULSAN NATIONAL INSTITUTE OF
SCIENCE AND TECHNOLOGY

Abstract

Alzheimer's disease (AD) is the most common cause of dementia. The symptoms of AD mainly include short-term memory loss, cognitive defects, and poor judgment, consequently leading to death. Currently 28 million people worldwide are suffering from AD; however, a cure for the disease to retard its initiation and progression has not been developed. Indeed, the discovery of the drug has been very challenging due to involvement of multiple pathogenic factors in the pathogenesis of AD. For example, the aggregates of amyloidogenic amyloid-β (Aβ) peptides are accumulated in the AD-affected brain. Among the aggregates, soluble and structured Aβ oligomers have been suggested to be toxic to nerve cells. Additionally, highly concentrated metal ions [*e.g.*, Cu(I/II), Zn(II), Fe(II/III)] are found in senile plaques, composed of Aβ aggregates. Disrupted homeostasis of these metal ions would affect neuron signaling, apoptosis, and inflammation. Lastly, reactive oxygen species (ROS) can be overproduced through Fenton-like reactions causing oxidative damage to nucleic acids and cellular organelles. The studies presented in this thesis describe the development of chemical tools able to regulate single or multiple pathogenic component(s). In Chapter 1, an introduction of the hypotheses of AD is described, along with previously reported chemical tools designed to target pathological elements. In Chapter 2, our interdisciplinary studies of new small molecules towards distinct pathological factors, rationally designed *via* a novel structure-property-directed design strategy, are summarized. Lastly, in Chapter 3, a series of fluorescent sensors for metal ions in living cells, is illustrated, which could provide a better understanding of a link of their concentration and compartmentalization to the pathogenesis of AD. Overall, our approaches and findings presented herein would be useful for constructing effective chemical tools and therapeutics for AD, ultimately serving the illumination of complex pathogenesis of the disease in the future.

ULSAN NATIONAL INSTITUTE OF
SCIENCE AND TECHNOLOGY

ULSAN NATIONAL INSTITUTE OF SCIENCE AND TECHNOLOGY

Table of Contents

Abstract…….....V
Table of Contents……...VI
List of Tables. …….....VIII
List of Figures.....IX
List of Schemes.....XIII
List of Abbreviations....…….....XIV

Chapter 1. Development of Chemical Tools Targeting Pathogenic Factors of Alzheimer's Disease to Elucidate its Complex Pathogenesis of the Disease

1.1. Introduction.....2
1.2. Hypotheses of AD.....2
1.2.1. Amyloid Hypothesis.....2
1.2.2. Metal Ion Hypothesis.....3
1.2.3. Oxidative Stress Hypothesis.....3
1.3. Development of Chemical Tools to Elucidate the Pathogeneses of AD.....4
1.3.1. Aβ-targeting Agents.....4
1.3.2. Metal Chelators.....5
1.3.3. Multifunctional Chemical Tools.....5
1.4. Conclusion.....6
1.5. References.....7

Chapter 2. Tuning Structures and Properties for Developing Novel Chemical Tools towards Distinct Pathogenic Elements in Alzheimer's Disease

2.1. Introduction.....11
2.2. Results and Discussion.....12
2.2.1. Structure-Property-Directed Principle for Designing Chemical Tools Able to Target Distinct Pathological Components of AD.....12
2.2.2. Synthesis and Characterization of **1**–**3**.....13
2.2.3. Redox Properties of **1**–**3**.....15
2.2.4. Interactions of **1**–**3** with Metal-free Aβ.....18
2.2.5. Interactions of **1**–**3** with Cu(II)–Aβ.....20
2.2.6. Regulatory Abilities of **1**–**3** against Metal-free Aβ and Metal–Aβ Aggregation……..23
2.2.7. Antioxidant Capabilities of **1**–**3** against Free Radicals.....25

ULSAN NATIONAL INSTITUTE OF SCIENCE AND TECHNOLOGY

2.3. Conclusions....27
2.4. Experimental Section....28
2.4.1. Materials and Methods....28
2.4.2. Preparation of **1**....28
2.4.3. Preparation of **2**....29
2.4.4. Preparation of **3**....30
2.4.5. Metal Binding Studies....30
2.4.6. Cyclic Voltammetry (CV)....30
2.4.7. DTNB Assay....31
2.4.8. Stability of Compounds....31
2.4.9. TEAC Assay....31
2.4.10. Aβ Aggregation Experiments....32
2.4.11. Gel Electrophoresis with Western Blotting....32
2.4.12. Transmission Electron Microscopy....32
2.4.13. MTT Assay....33
2.4.14. Electrospray Ionization Ion Mobility Mass Spectrometry....33
2.4.15. Parallel Artificial Membrane Permeability Assay Adapted for the Blood-brain Barrier (PAMPA–BBB).... 34
2.5. Acknowledgments....34
2.6. References....34
Chapter 3. Detection of Metal Ions in Living Cells by Fluorescence-based Chemosensors
3.1. Introduction....39
3.2. Results and Discussion....39
3.2.1. Fluorescent Responses of **AIC-Jul** to Al(III) in Living Cells....39
3.2.2. Fluorescent Responses of **TP-DAS** to Al(III) in Living Cells....40
3.2.3. Fluorescent Responses of **Sul-Nap** to Al(III) in Living Cells....41
3.3. Conclusions....42
3.4. Experimental Section....42
3.4.1. Imaging Experiments in Living Cells....42
3.5. Acknowledgments....43
3.6. References....43
Acknowledgments....44
Curriculum Vitae....45

ULSAN NATIONAL INSTITUTE OF
SCIENCE AND TECHNOLOGY

List of Tables

Table 2.1. Values (MW, *c*log*P*, HBA, HBD, PSA, logBB, and –logP_e) of **1**–**3**.

Table 2.2. Quantitative data of cyclic voltammograms of **1**–**3** in DMSO.

Table 2.3. Quantitative data of cyclic voltammograms of **1**–**3** in H_2O.

ULSAN NATIONAL INSTITUTE OF SCIENCE AND TECHNOLOGY

List of Figures

Figure 1.1. Production and aggregation of Aβ peptides. Aβ is generated by the proteolytic cleavage of APP *via* β- and γ-secretases. The Aβ monomers ($A\beta_{40}$ or $A\beta_{42}$) are prone to aggregate into oligomers, protofibrils, and fibrils.

Figure 1.2. Proposed mechanisms of Cu(I/II)–Aβ-mediated ROS production. Redox properties of Cu(I/II)–Aβ can direct the generation of H_2O_2 and •OH through the H_2O_2 cycle and Fenton cycle, respectively.

Figure 1.3. Aβ-targeting agents and metal chelators. (a and b) Structures of Aβ-targeting and their reaction mechanisms towards Aβ aggregations. (c) Structures of metal chelators.

Figure 1.4. Examples of multifunctional chemical tools towards Aβ, metal ions, and ROS. The structural moieties for Aβ interaction (highlighted in green), metal binding (highlighted in yellow), and radical scavenging (highlighted in blue) arer responsible for their activity towards pathogenic elements.

Figure 2.1. Rational design of the small molecules (**1**–**3**) able to have distinct properties and reactivities with pathological factors found in AD. (a and b) Structures of **DMA** and the bidentate ligands used for the construction of **1**–**3**. (c) Structural variations of **1**–**3**, obtained *via* a change of only one N or S donor atom in the framework, and the difference in their oxidation and targets.

Figure 2.2. ^{1}H (a, 400 MHz) and ^{13}C (b, 100 MHz) NMR spectra of **1** in CD_2Cl_2.

Figure 2.3. ^{1}H (a, 400 MHz) and ^{13}C (b, 100 MHz) NMR spectra of **2** in CD_2Cl_2.

Figure 2.4. ^{1}H (a, 400 MHz) and ^{13}C (b, 100 MHz) NMR spectra of **3** in CD_3OD.

Figure 2.5. Metal binding of **1**–**3** observed by UV–Vis. Spectral changes of our molecules are monitored upon titration of various concentrations of (a) Cu(II) and (b) Zn(II). Conditions: [compound] = 50 μM, [$CuCl_2$ or $Zn(NO_3)_2$] = 0 (blue), 25, 50, 100, and 250 μM (orange), EtOH [for Cu(II) binding studies] or buffered solution [20 μM HEPES, pH 7.4, 150 μM NaCl, for Zn(II) binding studies], room temperature, incubation for 10 min.

ULSAN NATIONAL INSTITUTE OF SCIENCE AND TECHNOLOGY

Figure 2.6. Redox potentials of **1**–**3** measured in DMSO. The oxidation of (a) **1**–**3** and (b) their structural portions was monitored by cyclic voltammetry. The E_{pa} values at 250 mV/s are summarized in (c). Conditions: [compound] = 1 mM; 0.1 M *tetra-N*-butylammonium perchlorate (in DMSO); various scan rates [25 (red), 50, 100, 150, 200, and 250 mV/s (blue)]; room temperature; three electrodes composed of the glassy carbon working electrode, platinum counter electrode, and Ag/Ag(I) reference electrode.

Figure 2.7. Redox potentials of **1**–**3** measured in H_2O. The oxidation of **1**, **3**, and **DMPD** was monitored by cyclic voltammetry. Conditions: [compound] = 1 mM; 1 M NaCl (in ddH_2O); various scan rates [25 (red), 50, 100, 150, 200, and 250 mV/s (blue)]; room temperature; three electrodes composed of the glassy carbon working electrode, platinum counter electrode, and Ag/Ag(I) reference electrode.

Figure 2.8. Oxidation of thiol groups in *L*-cysteine (*L*-Cys) and compounds, monitored by the DTNB assay. *L*-Cys was used as a positive control in the DTNB assay. Conditions: [DTNB] = 50 μM; [compound] = 50 μM; buffered solution (pH 8.0); room temperature; incubation for 10 min.

Figure 2.9. Oxidation of **1**–**3** monitored by UV–Vis. Conditions: [compound] = 50 μM; 20 μM HEPES, pH 7.4, 150 μM NaCl; room temperature; incubation for 24 h.

Figure 2.10. Interactions of **1**–**3** with metal-free $A\beta_{40}$, analyzed by ESI–MS and ESI–MS^2. (a) The +3-charged $A\beta_{40}$ monomers in the samples incubated with **1**–**3** in the absence of Cu(II) were detected in the ESI–MS spectra. Metal-free $A\beta_{40}$ is denoted as red peaks. The oxidized ions are indicated by the red asterisks. (b) The oxidized amino acid residue of $A\beta_{40}$ incubated with **1** was identified through ESI–MS^2. Conditions: [$A\beta_{40}$] = 100 μM; [compound] = 500 μM; incubation for 3 h; 20 mM ammonium acetate, pH 7.2; 37 °C; no agitation. All samples were diluted with ddH_2O by 10 fold before injection to the mass spectrometer.

Figure 2.11. Interactions of **1**–**3** with Cu(II)-treated $A\beta_{40}$, analyzed by ESI–MS and ESI–MS^2. (a) The +3-charged $A\beta_{40}$ monomers in the samples incubated with **1**–**3** in the presence of Cu(II) were detected in the ESI–MS spectra. Cu(II)–$A\beta_{40}$ is denoted as light blue peaks, respectively. The oxidized ions are indicated by the red asterisks. The number of the asterisks represents the number of the oxygen atoms incorporated into $A\beta_{40}$. The degraded $A\beta_{40}$ with 89 Da loss (orange peaks) was presented from the **1**-

ULSAN NATIONAL INSTITUTE OF SCIENCE AND TECHNOLOGY

treated samples in the presence of Cu(II). (b) The oxidized amino acid residues of $A\beta_{40}$ incubated with **1** and Cu(II) were identified through ESI–MS^2. Conditions: [$A\beta_{40}$] = 100 μM; [$CuCl_2$] = 100 μM; [compound] = 500 μM; incubation for 1 h; 20 mM ammonium acetate, pH 7.2; 37 °C; no agitation. All samples were diluted with ddH_2O by 10 fold before injection to the mass spectrometer.

Figure 2.12. Interactions of **2** with Cu(II)-treated monitored $A\beta_{42}$ monitored by ESI–MS and IM–MS. (a) The +5-charged Cu(II)-treated $A\beta_{42}$ dimer in the samples incubated without (left) or with **2** (right). The non-covalent complex formation of **BT** (153 *m/z*) or $\mathbf{BT_{ox}}$ (304 *m/z*) with $A\beta_{42}$ was detected in the ESI–MS spectra (green peak, 1868 *m/z*). (b) The altered arrival time distributions (ATDs) of Cu(II)–$A\beta_{42}$ upon incubation with **2** indicate the conformational change of the peptide. Ions selected for the IM–MS analysis are marked with gray and orange circles in the ESI–MS spectra. Conditions: [$A\beta_{42}$] = 100 μM; [$CuCl_2$] = 100 μM; [**2**] = 500 μM; incubation for 1 h; 20 mM ammonium acetate, pH 7.2; 37 °C; no agitation. All samples were diluted with ddH_2O by 10 fold before injection to the mass spectrometer

Figure 2.13. Reactivities of **1**–**3** to inhibit metal-free Aβ and metal–Aβ aggregation. (a) Scheme of the inhibition experiments. (b) Analysis of the size distributions of the resultant $A\beta_{40}$ and $A\beta_{42}$ species from (a) by gel/Western blot using 6E10. (**C**) [Aβ ± Cu(II) or Zn(II)]; (**1**) [(C) + **1**]; (**2**) [(C) + **2**]; (**3**) [(C) + **3**]. Conditions: [Aβ] = 25 μM; [$CuCl_2$ or $ZnCl_2$] = 25 μM; [compound] = 50 μM; pH 6.6 [for Cu(II) samples] or pH 7.4 [for metal-free and Zn(II) samples]; 37 °C; constant agitation. (c) TEM images of the samples from (b). The inset image represents the minor species. Scale bar = 200 nm.

Figure 2.14. Reactivities of **1**–**3** against the preformed metal-free Aβ and metal–Aβ aggregates. (a) Scheme of the disaggregation experiments. (b) Analysis of the size distributions of the resultant $A\beta_{40}$ and $A\beta_{42}$ species from (a) by gel/Western blot using 6E10. (**C**) [Aβ ± Cu(II) or Zn(II)]; (**1**) [(C) + **1**]; (**2**) [(C) + **2**]; (**3**) [(C) + **3**]. Conditions: [Aβ] = 25 μM; [$CuCl_2$ or $ZnCl_2$] = 25 μM; [compound] = 50 μM; pH 6.6 [for Cu(II) samples] or pH 7.4 [for metal-free and Zn(II) samples]; 37 °C; constant agitation. (c) TEM images of the resultant $A\beta_{40}$/$A\beta_{42}$ aggregates from the 24 h incubated samples from (b). Scale bar = 200 nm.

Figure 2.15. Scavenging capability of **1**–**3** against free organic radicals in N2a cell lysates, determined by the TEAC assay. The TEAC values of compounds are summarized in (b). *n.d., not determined. The TEAC values of ethanamine (**EA**) and ethanethiol (**ET**) were not able to be obtained due to their limited activity.

ULSAN NATIONAL INSTITUTE OF SCIENCE AND TECHNOLOGY

Figure 2.16. Toxicity of compounds in SH-SY5Y (5Y) cells. (a) Cell survival of compounds (**1**–**3**) in the absence of metal ions. (b) Cell survival of compounds (*i.e.,* **1** and **2**) in the presence of metal ions. (c) Cell survival of compounds (*i.e.,* **1** and **2**) in the presence of $A\beta_{40}$ or $A\beta_{42}$ and metal ions. Conditions: [Aβ] = 10 μM; [$CuCl_2$ or $ZnCl_2$] = 5 μM; [compound] = 10 μM.

Figure 3.1. Fluorescent responses of **AIC-Jul** to Al(III) in HeLa cells in the absence and presence of PPi. (a) Cells were pre-incubated with **AIC-Jul** for 10 min prior to addition of various concentrations of Al(III). (b) Cells incubated with **AIC-Jul** (for 5 min) followed by addition of Al(III) for 10 min were treated with various concentrations of PPi. Conditions: [**AIC-jul**] = 20 μM; [Al(III)] = 0, 100, and 200 μM; [PPi] = 0, 100, and 200 μM; 37 °C; 5% CO_2. The scale bar is 50 μm.

Figure 3.2. Fluorescent response of **TP-DAS** to Al(III) in HeLa cells. Cells were pre-incubated with **TP-DAS** for 10 min prior to addition of various concentrations of Al(III). Conditions: [**TP-DAS**] = 5 μM; [Al(III)] = 0, 100, 200, and 300 μM; 37 °C; 5% CO_2. The scale bar is 50 μm.

Figure 3.3. Fluorescent responses of **Sul-Nap** to Al(III) in HeLa cells. Cells were pre-incubated with **Sul-Nap** for 10 min prior to addition of Al(III). Conditions: [**Sul-Nap**] = 20 μM; [Al(III)] = 100 μM; 37 C; 5% CO_2. Scale bar = 50 μm.

ULSAN NATIONAL INSTITUTE OF SCIENCE AND TECHNOLOGY

List of Schemes

Scheme 2.1. Synthetic routes to **1**–**3**.

Scheme 2.2. Reaction scheme of the DTNB assay

Scheme 3.1. Proposed structure of the **AIC-jul**–Al(III) complex.

Scheme 3.2. Proposed structure of the **TP-DAS**–Al(III) complex.

Scheme 3.3. Proposed structure of the **Sul-Nap**–Al(III) complex.

ULSAN NATIONAL INSTITUTE OF SCIENCE AND TECHNOLOGY

List of Abbreviations

Aβ	Amyloid-β
ABTS	2,2'-Azino*bis*-(3-ethylbenzothiazoline-6-sulfonic acid)
AD	Alzheimer's disease
AMPA	α-Amino-3-hydroxy-5-methyl-4-isoxazolepropionate
APH1	Anterior pharynx
APP	Amyloid precursor protein
Asp	Aspartate
ATP	Adenosine triphosphate
BBB	Blood-brain barrier
BT	4-(Dimethylamino)benzenethiol
CQ	Clioquinol
DAPI	2-(4-Amidinophenyl)-1*H*-indole-6-carboxamidine
DMA	*N*,*N*-Dimethylaniline
DMPD	*N*,*N*-Dimethyl-*p*-phenylenediamine
DMSO	Dimethyl sulfoxide
DTNB	5,5'-Dithio-*bis*-(2-nitrobenzoic acid)
CV	Cyclic voltammetry
EA	Ethanamine
E_{pa}	Anodic peak potential
ESI–MS	Electrospray ionization mass spectrometry
ET	Ethanethiol
FDA	Food and Drug Administration
GFP	Green fluorescence protein
HIF	Hypoxia-inducible factors
His	Histidine

ULSAN NATIONAL INSTITUTE OF SCIENCE AND TECHNOLOGY

IM–MS	Ion mobility mass spectrometry
L-Cys	*L*-Cysteine
Met	Methionine
Metal–Aβ	Metal-bound Aβ
MS	Mass spectrometry
MW	Molecular weight
NHE	Normal hydrogen electrode
NMDA	*N*-methyl-D-aspartate
NMR	Nuclear magnetic resonance
PD	Parkinson's disease
PEN2	Presenilin enhancer 2
PET	Positron emission topography
PIB	Pittsburgh compound B
PPi	Pyrophosphate
ROS	Reactive oxygen species
SOD	Superoxide dismutase
TEAC	Trolox equivalent antioxidant capacity
TEM	Transmission electron microscopy
ThT	Thioflavin-T
TNB^{2-}	2-Nitro-5-thiobenzoic acid dianion
UV–Vis	UV-visible spectrophotometer

ULSAN NATIONAL INSTITUTE OF
SCIENCE AND TECHNOLOGY

Chapter 1.

Development of Chemical Tools Targeting Pathogenic Factors of Alzheimer's Disease to Elucidate its Complex Pathogenesis of the Disease

1.1. Introduction

Alzheimer's disease (AD) is the most common neurodegenerative disease, estimated approximately 60-80% of dementia.[1] The disease was first reported in 1906;[1] however, the etiology of the disease has not still been clear.[2-4] The main symptoms of the disease include loss of episodic memory, cognitive decline, disorientation, and poor judgment, which could ultimately lead to death.[1,5] The hallmarks of AD consist of senile plaques and neurofibrillary tangles, mostly composed of amyloid-β (Aβ) aggregates and hyperphosphorylated tau (ptau) protein, respectively.[5-8] The Alzheimer's Association reported that the resultant social cost per patient for health care and long-term care services hovers at approximately 50 million won annually.[1] Although 28 million people worldwide are currently suffered by the disease, a few medications (*e.g.*, donepezil, memantine, galantamine, and rivastigmine), approved by the U.S. Food and Drug Administration (FDA), are available but they provide only temporary symptom relief by blocking a single risk factor, cholinesterase or *N*-methyl-D-aspartate (NMDA) receptor.[1,3] Until now, due to the complexity of AD pathology, a cure for the disease has not been successfully developed. In this Chapter, we illustrate the representative pathological factors of AD and their inter-relationships. In addition, some previously reported chemical tools able to target and modulate such elements are presented.

1.2. Hypotheses of AD

1.2.1. Amyloid Cascade Hypothesis

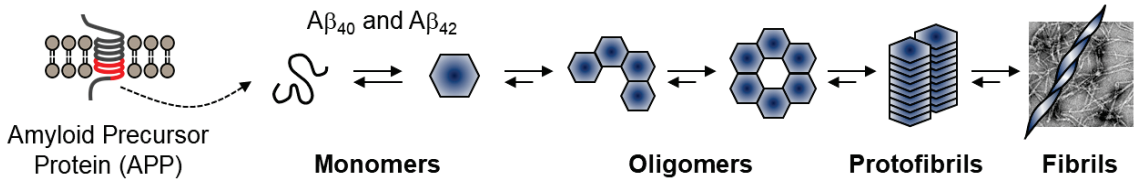

Figure 1.1. Production and aggregation of Aβ peptides. Aβ is generated by the proteolytic cleavage of APP *via* β- and γ-secretases. The Aβ monomers ($A\beta_{40}$ or $A\beta_{42}$) are prone to aggregate into oligomers, protofibrils, and fibrils.

In order to invent an effective treatment for AD, the etiology of the disease needs to be first identified. Multiple risk factors of AD have been suggested through several hypotheses: the amyloid cascade hypothesis, metal ion hypothesis, and the oxidative stress hypothesis.[2-5,9,10] Amyloid hypothesis claims that the aggregation of misfolded Aβ proteins is relevant to the neurotoxicity in AD.[2,4,5,10] Aβ peptides are generated *via* the proteolytic cleavage of amyloid precursor protein (APP) by β- and γ-secretases.[5,11] The isoforms of Aβ peptides are determined depending on the cleavage site of γ-secretase.[5,11] $A\beta_{40}$ and $A\beta_{42}$ are the dominant products from the cleavage reactions with the difference in two hydrophobic amino acid residues (*i.e.*, isoleucine and alanine) in the C-terminus.[4,5,11] Aβ

ULSAN NATIONAL INSTITUTE OF SCIENCE AND TECHNOLOGY

monomers are natively disordered; however, external factors, such as pH and temperature, cause peptides to be partially folded,[11] which tend to spontaneously aggregate into oligomers, protofibrils, and fibrils (Figure 1.1).[2,3,5-7] Among various species, structured soluble Aβ oligomers are recently reported to be the most toxic species which could disrupt cellular signaling pathways by interfering membrane receptors [*e.g.*, α-amino-3-hydroxy-5-methyl-4-isoxazolepropionate (AMPA) receptor and NMDA receptor] or forming annular structures inserted in the membrane.[8,11]

1.2.2. Metal Ion Hypothesis

Homeostasis of transition metal ions, including Cu(I/II) and Zn(II), are impaired in the AD-affected brain.[4,5,12-14] Since metal ions are responsible for numerous signal transduction pathways including apoptosis, inflammation, and cell proliferation, dysregulated metal ions are also pathogenic.[4] In general, the concentrations of intracellular Cu(I/II) and Zn(II) are tightly regulated by various metal transporters (*e.g.*, ATP7A and ATP7B for copper;[4,15] ZnT3 for zinc[4,16]). Under pathological conditions, however, such metal ions are not properly compartmentalized in the regions of the brain (*e.g.*, hippocampus, cortex, amygdala, and putamen).[4] For example, the deficiency and overload of Cu(I/II) are simultaneously observed in the hippocampus and putamen of AD patients.[17,18] The loss of protein-bound metal ions in metalloenzymes [*e.g.*, cytochrome c oxidase and Cu/Zn-superoxide dismutase (SOD)] can influence neuron degeneration and apoptosis.[5] In addition to the effects of metal ions on the activities of metalloenzymes, they can form 1:1 complexes with the peptide [$K_d = 10^{-11}$ to 10^{-8} M for Cu(II); $K_d = 10^{-9}$ to 10^{-6} M for Zn(II)], which facilitates Aβ aggregation and stabilizes toxic oligomeric species.[4,13,14,19] The exact mechanisms of how metal ions could affect the aggregation pathways of Aβ have not been identified.[13]

1.2.3. Oxidative Stress Hypothesis

The overproduction of reactive oxygen species (ROS) can trigger damage to the nucleic acid, membranes, and cellular organelles, consequently leading to neuronal death.[5,12,20] The oxidative stress hypothesis proposes that the sources of ROS could be hypoxia and amyloid-related events.[5,21] First, the condition of hypoxia stimulates the respiratory system in mitochondria, reducing dioxygen (O_2) to superoxide ($O_2^{\bullet-}$), that prompts oxidative stress through overexpression of hypoxia-inducible factors (HIFs).[22] Under hypoxia conditions, however, HIFs cannot be degraded;[23] thus, the oxidative damages are further amplified through positive feedback.

In addition, as described above, dysregulated metal ions can bind to Aβ, generating metal–Aβ complexes (*vide supra*). Particularly, redox-active Cu(II)–Aβ could generate hydrogen peroxide (H_2O_2) through the H_2O_2 cycle (Figure 1.2)[5,7,9,24] upon reduction from Cu(II) to Cu(I), with a half potential as 0.34 V [*versus* normal hydrogen electrode (NHE)].[25] Moreover, in the presence of

ULSAN NATIONAL INSTITUTE OF SCIENCE AND TECHNOLOGY

reducing agents, such as ascorbic acids or glutathione,[7,25] Cu(I)–Aβ additionally cleaves the O–O bond of H_2O_2 to generate hydroxyl radicals (•OH) through Fenton-like reactions (Figure 1.2).[5,7,9,24] ROS-mediated oxidative stress can be controlled *via* mitochondrial detoxifying mechanisms (*i.e.*, SOD and catalase) under normal conditions;[2] however, abnormal mitochondria in the AD-affected brain are able to overproduce $O_2^{\bullet-}$ and release H_2O_2 into the cytoplasm.[2,5]

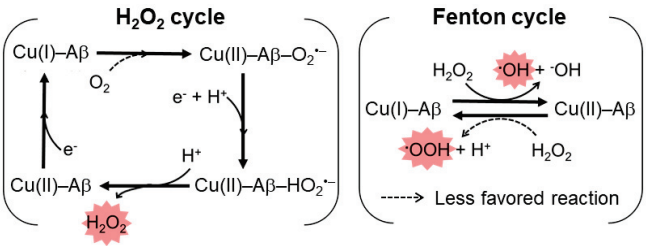

Figure 1.2. Proposed mechanisms of Cu(I/II)–Aβ-mediated ROS production. Redox properties of Cu(I/II)–Aβ can direct the generation of H_2O_2 and •OH through the H_2O_2 cycle and Fenton cycle, respectively.

1.3. Development of Chemical Tools to Elucidate the Pathogeneses of AD

1.3.1. Aβ-targeting Agents

In order to identify the role of Aβ aggregation in the neurotoxicity,[2,4,5,10] chemical tools capable of targeting and regulating them would be necessary. For example, thioflavin-T (**ThT**) and Pittsburgh compound B (**PIB**) derivatives have been utilized to interact with β-sheet-enriched amyloid aggregates *in vivo* (Figure 1.3.a).[2,4] In addition, some Aβ antibodies (*e.g.*, bapineuzumab, solanezumab, ponezumab) are undergoing Phase III clinical trials, which can specifically bind to certain Aβ sequences and lower the levels of Aβ in the brain of AD patients.[27] Moreover, the inhibitors against γ-secretase, composed of at least four proteins [*i.e.*, presenilin, nicastrin, anterior pharynx (APH1), and presenilin enhancer 2 (PEN2)], were developed to completely prevent the generation of Aβ peptides.[3,28,29] Unfortunately, γ-secretase has other substrates (*e.g.*, notch receptor 1) rather than APP; thus, suppression of this secretase could cause notch-related lethal side effects.[29,30] As an alternative approach, small molecules able to modulate Aβ aggregation into off-pathway have been developed.[29,31] For instance, β-sheet breakers have been recently proposed to inhibit or disrupt the formation of β-sheet by binding to the self-recognition site of Aβ species (Figure 1.3.b).[29,31] In an inverse direction, Wanker and coworkers have reported the molecule, **O4**, that could interact with hydrophobic residues of Aβ and accelerates Aβ fibrillization leading to reduction of the amount of toxic oligomers (Figure 1.3.b).[32]

ULSAN NATIONAL INSTITUTE OF SCIENCE AND TECHNOLOGY

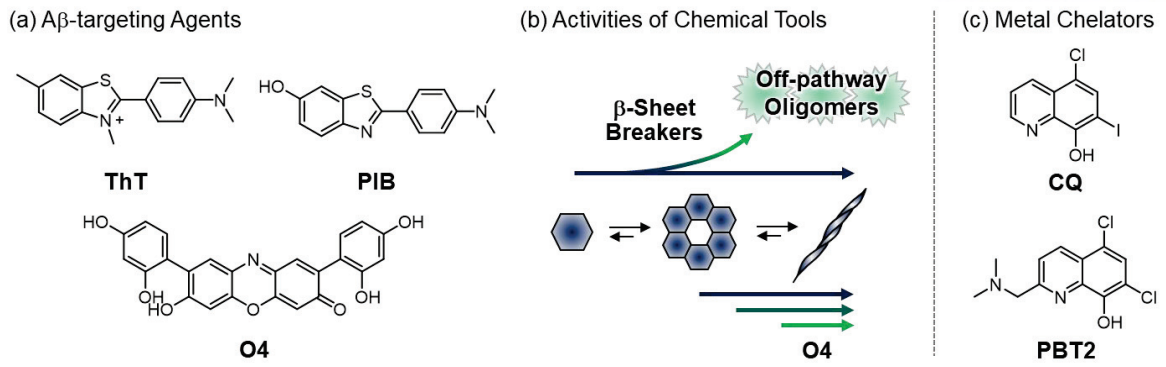

Figure 1.3. Aβ-targeting agents and metal chelators. (a and b) Structures of Aβ-targeting and their reaction mechanisms towards Aβ aggregations. (c) Structures of metal chelators.

1.3.2. Metal Chelators

In order to redistribute abnormally compartmentalized metal ions in the AD-affected brain, effective metal chelators possessing reasonable binding affinities towards Cu(II), Zn(II), and Fe(II/III) are necessary. At the same time, metal binding affinities of chemical tools should be adjusted to avoid stripping out the essential biometals in metalloproteins.[8] Moreover, since metal ions have been known to directly bind Aβ species as well as overproduce ROS, chemical reagents able to attenuate the interactions between metal ions and the peptide would be valuable.[4,8] Clioquinol (**CQ**) is the common example of metal chelators utilized as an AD therapeutics (specifically, chelation of Cu(II) and Zn(II) [K_d = 10^{-10} M for Cu(II); 10^{-8} M for Zn(II)] as well as decrease in the level of Aβ in the brain of AD patients (Figure 1.3.c).[3,33,34] Due to the toxicity of impurity (*i.e.*, 5,7-diiodoquinolin-8-ol) generated during mass production, however, further clinical trials were halted. As a derivative of **CQ**, **PBT2** was shown to function same as **CQ**, along with greater blood-brain barrier (BBB) permeability (Figure 1.3.c).[3,34,35] Moreover, both **CQ** and **PBT2** are shown to reorganize the disturbed homeostasis of metal ions and activate metalloenzymes responsible for Aβ clearance (*i.e.*, MMP-2 and MMP-3).[3,35]

1.3.3. Multifunctional Chemical Tools

Given that various risk factors found in AD are intertwined with one another (*vide supra*), the development of multifunctional chemical tools towards several elements (*i.e.*, Aβ, metal ions, metal–Aβ, and ROS) has recently received significant attention. **Cyc-KLVFF**, one of the cyclen derivatives incorporated to the amino acid residues in the self-recognition site of Aβ, has shown its novel ability to chelate Cu(II) and break the β-sheets as designed as a dual-functional chemical tool (Figure 1.4).[36] Interestingly, this molecule could further decrease H_2O_2 production mediated by Cu(II)–$A\beta_{42}$.[36] As described in the previous section, the dyshomeostasis of redox-active metal ions is closely correlated with overproduction of ROS;[5,7,9,24] thus, **Cyc-KLVFF** can function as an antioxidant by preventing the

ULSAN NATIONAL INSTITUTE OF SCIENCE AND TECHNOLOGY

oxidative damages induced by ROS.[36] Additionally, our group has reported the molecule, **ML**, composed of rationally chosen structural moieties responsible for interacting with metal-free Aβ, metal-bound Aβ, and metal ions as well as scavenging free radicals (Figure 1.4).[10] The framework of **ML** is based on *p*-I-stilbene[37] and **L2-b**,[38] each of which is a well-known Aβ imaging agent and a previously reported small molecule targeting metal–Aβ, respectively. In order to afford a tetradentate ligand with a relatively high metal binding affinity,[39] an additional hydroxyl group was incorporated into the framework. The distorted square planar geometry of the Cu(II)–**ML** complex is indicated, which is not favorable for the geometry of Cu(I)–**ML** and thus subsequently prevents ROS generation *via* Fenton-like reactions.[5,7,9,24] Moreover, it contains the moieties of quinoline and phenol that are previously reported to scavenge free radicals.[10] **ML** could redirect the aggregation pathways of both metal-free Aβ and metal–Aβ as well as regulate the levels of ROS (*i.e.*, inhibition of forming ROS and scavenging of the free radicals). In addition to the rationally designed molecules, natural products have been investigated to function as multifunctional tools. For example, melatonin, a hormone responsible for maintaining the circadian rhythm, is a well-known antioxidant.[40] The amide functional group of melatonin could contribute to the interaction with Cu(II) and Zn(II),[40] inhibiting the formation of metal–Aβ oligomers (Figure 1.4).[41] Vitamine E (α-tocopherol) was observed to inhibit Aβ aggregation as well as disaggregate preformed Aβ fibrils along with its antioxidant capacity (Figure 1.4).[42]

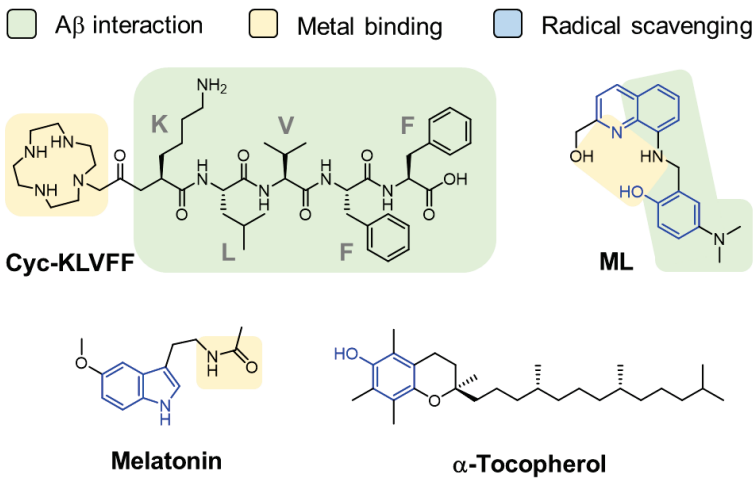

Figure 1.4. Examples of multifunctional chemical tools towards Aβ, metal ions, and ROS. The structural moieties for Aβ interaction (highlighted in green), metal binding (highlighted in yellow), and radical scavenging (highlighted in blue) arer responsible for their activity towards pathogenic elements.

1.4. Conclusions

A growing number of AD patients is emerging as a severe social problem; however, the clear

ULSAN NATIONAL INSTITUTE OF SCIENCE AND TECHNOLOGY

medication has not been provided. Multiple pathological factors, including Aβ, metal ions, and ROS, are found in the AD-affected brain. These pathogenic factors are observed to be closely inter-related with one another, aggravating the neurotoxicity. In order to advance our understanding of the complicated pathology of AD and provide a new insight into the discovery of therapeutics, the development of chemical tools towards modulation of such pathological components would be necessary. In this Chapter, we illustrate some examples of chemical reagents, including Aβ-targeting agents, metal chelators, and multifunctional chemical tools.

1.5. References

1. Alzheimer's Association, *Alzheimers Dement.* **2017**, *13*, 325–373.
2. Jakob-Roetne, R.; Jacobsen, H. *Angew. Chem. Int. Ed.* **2009**, *48*, 3030–3059.
3. Derrick, J. S.; Lim, M. H. *ChemBioChem* **2015**, *16*, 887–898.
4. Kepp, K. P. *Coord. Chem. Rev.* **2017**, *351*, 127–159.
5. Kepp, K. P. *Chem. Rev.* **2012**, *112*, 5193–5239.
6. DeToma, A. S.; Salamekh, S.; Ramamoorthy, A.; Lim, M. H. *Chem. Soc. Rev.* **2012**, *41*, 608–621.
7. Savelieff, M. G.; Lee, S.; Liu, Y.; Lim, M. H. *ACS Chem. Biol.* **2013**, *8*, 856–865.
8. Hamley, I. W. *Chem. Rev.* **2012**, *112*, 5147–5239.
9. Rauk, A. *Chem. Soc. Rev.* **2009**, *38*, 2698–2715.
10. Lee, S.; Zheng, X.; Krishnamoorthy, J.; Savelieff, M. G.; Park, H. M.; Brender, J. R.; Kim, J. H.; Derrick, J. S.; Kochi, A.; Lee, H. J.; Kim, C.; Ramamoorthy, A.; Bowers, M. T.; Lim, M. H. *J. Am. Chem. Soc.* **2014**, *136*, 299–310.
11. Lee, S. J. C.; Nam, E.; Lee, H. J.; Savelieff, M. G.; Lim, M. H. *Chem. Soc. Rev.* **2017**, *46*, 310–323.
12. Smith, D. G.; Cappai, R.; Barnham, K. J. *Biochim. Biophys. Acta.* **2007**, *1768*, 1976–1990.
13. Faller, P.; Hureau, C.; Berthoumieu, O. *Inorg. Chem.* **2013**, *52*, 12193–12206.
14. Faller, P.; Hureau, C. *Dalton Trans.* **2009**, *7*, 1080–1094.
15. Waggoner, D. J.; Bartnikas, T. B.; Gitlin, J. D. *Neurobiol. Dis.* **1999**, *6*, 221–230.
16. Zhang, M.; Zhou, H.; He, R.; Di, F.; Yang, L.; Yang, T. *Endocrine* **2010**, *37*, 241–243.
17. Deibel, M. A.; Ehmann, W. D.; Markesbery, W. R. *J. Neurol. Sci.* **1996**, *143*, 137–142.
18. Andrasi, E.; Farkas, E.; Gawlik, D.; Rosick, U.; Bratter, P. *J. Alzheimers Dis.* **2000**, *2*, 17–26.
19. Hureau, C.; Faller, P. *Biochimie* **2009**, *91*, 1212–1217.
20. Markesbery, W. R. *Free Radic. Biol. Med.* **1997**, *23*, 134–147.
21. Zhu, X.; Raina, A. K.; Perry, G.; Smith, M. A. *Lancet. Neurol.* **2004**, *3*, 219–226.
22. Chandel, N. S.; Budinger, G. R. *Free Radic. Biol. Med.* **2007**, *42*, 165–174.

ULSAN NATIONAL INSTITUTE OF SCIENCE AND TECHNOLOGY

23. Berra, E.; Benizri, E.; Ginouves, A.; Volmat, V.; Roux, D.; Pouyssegur, J. *EMBO J.* **2003**, 22, 4082–4090.
24. Jomova, K.; Vondrakova, D.; Lawson, M.; Valko, M. *Mol. Cell. Biochem.* **2010**, *345*, 91–104.
25. Guilloreau, L.; Combalbert, S.; Sournia-Saquet, A.; Mazarguil, H.; Faller, P. *ChemBioChem* **2007**, *8*, 1317–1325.
26. Klunk, W. E.; Engler, H.; Nordberg, A.; Wang, Y.; Blomqvist, G.; Holt, D. P.; Bergstrom, M.; Savitcheva, I.; Huang, G. F.; Estrada, S.; Ausen, B.; Debnath, M. L.; Barletta, J.; Price, J. C.; Sandell, J.; Lopresti, B. J.; Wall, A.; Koivisto, P.; Antoni, G.; Mathis, C. A.; Langstrom, B. *Ann. Neurol.* **2004**, *55*, 306–319.
27. Karran, E.; Hardy, J. *Ann. Neurol.* **2014**, *76*, 185–205.
28. Panza, F.; Solfrizzi, V.; Frisardi, V.; Capurso, C.; D'Introno, A.; Colacicco, A. M.; Vendemiale, G.; Capurso, A.; Imbimbo, B. P. *Drugs Aging* **2009**, *26*, 537–555.
29. Hamaguchi, T.; Ono, K.; Yamada, M. *Cell. Mol. Life Sci.* **2006**, *63*, 1538–1552.
30. De Strooper, B.; Annaert, W.; Cupers, P.; Saftig, P.; Craessaerts, K.; Mumm, J. S.; Schroeter, E. H.; Schrijvers, V.; Wolfe, M. S.; Ray, W. J.; Goate, A.; Kopan, R. *Nature* **1999**, *398*, 518–522.
31. Lorenzo, A.; Yankner, B. A. *Proc. Natl. Acad. Sci. U. S. A.* **1994**, *91*, 12243–12247.
32. Bieschke, J.; Herbst, M.; Wiglenda, T.; Friedrich, R.; Boeddrich, A.; Shiele, F.; Kleckers, D.; del Amo, J. M. L.; Gruning, B. A.; Wang, Q.; Schmidt, M. R.; Lurz, R.; Anwyl, R.; Schnoegl, S.; Fandrich, M.; Frank, R. F.; Reif, B.; Gunther, S.; Walsh, D.; Wanker, E. E. *Nat. Chem. Biol.* **2012**, *8,* 93–101.
33. Bush, A. I.; Tanzi, R. E. *Neurotherapeutics* **2008**, *5*, 421–432.
34. Relkin, N. R. *Lancet. Neurol.* **2008**, *7*, 762–763.
35. Adlard, P. A.; Cherny, R. A.; Finkelstein, D. I.; Gautier, E.; Robb, E.; Cortes, M.; Volitakis, I.; Liu, X.; Smith, J. P.; Perez, K.; Laughton, K.; Li, Q. X.; Charman, S. A.; Nicolazzo, J. A.; Wilkins, S.; Deleva, K.; Lynch, T.; Kok, G.; Ritchie, C. W.; Tanzi, R. E.; Cappai, R.; Masters, C. L.; Barnham, K. J.; Bush, A. I. *Neuron* **2008**, *59*, 43–55.
36. Wu, W. H.; Lei, P.; Liu, Q.; Hu, J.; Gunn, A. P.; Chen, M. S.; Rui, Y. F.; Su, X. Y.; Xie, Z. P.; Zhao, Y. F.; Bush, A. I.; Li, Y. M. *J. Biol. Chem.* **2008**, *283*, 31657–31664.
37. Kung, H. F.; Lee, C. W.; Zhuang, Z. P.; Kung, M. P.; Hou, C.; Plossl, K. *J. Am. Chem. Soc.* **2001**, *123*, 12740–12741.
38. Choi, J. S.; Braymer, J. J.; Nanga, R. P.; Ramamoorthy, A.; Lim, M. H. *Proc. Natl. Acad. Sci. U. S. A.* **2010**, *107*, 21990–21995.
39. Lim, M. H.; Wong, B. A.; Pitcock, W. H., Jr.; Mokshagundam, D.; Baik, M. H.; Lippard, S. J. *J. Am. Chem. Soc.* **2006**, *128*, 14364–14373.
40. Limson, J.; Nyokong, T.; Daya, S. *J. Pineal. Res.* **1998**, 24, 15–21.

ULSAN NATIONAL INSTITUTE OF
SCIENCE AND TECHNOLOGY

41. Pappolla, M.; Bozner, P.; Soto, C.; Shao, H.; Robakis, N. K.; Zagorski, M.; Frangione, B.; Ghiso, J. *J. Biol. Chem.* **1998**, *273*, 7185–7188.

42. Yang, S. G.; Wang, W. Y.; Ling, T. J.; Feng, Y.; Du, X. T.; Zhang, X.; Sun, X. X.; Zhao, M.; Xue, D.; Yang, Y.; Liu, R. T. *Neurochem. Int.* **2010**, *57*, 914–922.

ULSAN NATIONAL INSTITUTE OF SCIENCE AND TECHNOLOGY

Chapter 2.

Tuning Structures and Properties for Developing Novel Chemical Tools towards Distinct Pathogenic Elements in Alzheimer's Disease

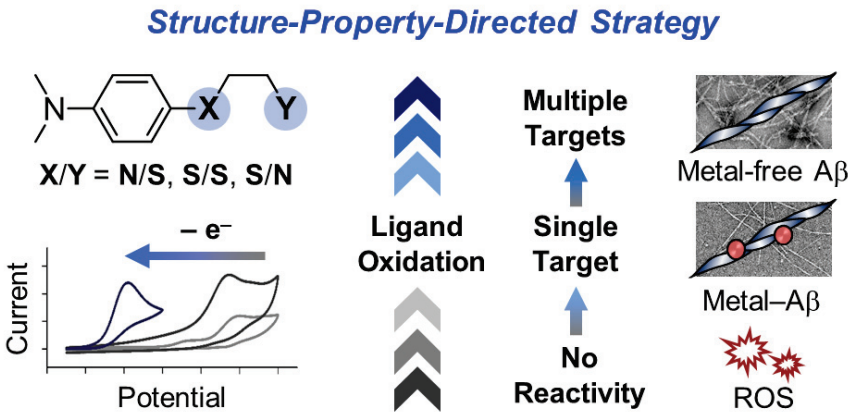

I thank Dr. Hyuck Jin Lee for the studies of TEM, gel/Western blot, and cells; Kyu Yeon Kim and Professor Junghyun Chae for the synthesis of the small molecules (**1**–**3**); Dr. Shin Jung C. Lee for helping the analysis of mass spectrometric data. I carried out the experiments using cyclic voltammetry, UV–visible spectroscopy, biochemical assays (PAMPA–BBB, DTNB assay, and TEAC assay), analyses of mass spectrometry, gel/Western blot, and living cells along with data analyses.

ULSAN NATIONAL INSTITUTE OF SCIENCE AND TECHNOLOGY

2.1 Introduction

Various pathological factors [*e.g.*, amyloid-β (Aβ), metal ions, metal-bound Aβ (metal–Aβ), reactive oxygen species (ROS)] are reported to be involved in the pathogenesis of Alzheimer's disease (AD).[1-10] Aβ peptides, produced *via* the proteolytic cleavage of amyloid precursor protein (APP), tend to aggregate into oligomers, protofibrils, and fibrils.[1,2,8-10] Recently, soluble Aβ oligomers are suggested to be major toxic species that cause neuronal atrophy and death.[2,10-13] Additionally, highly concentrated metals (*e.g.*, copper, zinc, iron) found in senile plaques are observed to directly interact with Aβ generating metal–Aβ complexes, which can facilitate Aβ aggregation and stabilize toxic Aβ oligomers.[8,13-15] Moreover, complexes of Aβ and redox-active metal ions, including Cu(I/II), are presented to overproduce ROS *via* Fenton-like reactions leading to damage of nucleic acids, lipids, and cellular organelles.[2,16-18] Due to the complex link among multiple pathological elements to AD pathology, however, a cure for the disease has not been still discovered.[8,19]

In order to gain a better understanding of the pathogenesis of AD, chemical tools capable of targeting and modulating pathogenic factors have been devised.[20-39] A variety of anti-amyloidogenic compounds that interact with metal-free Aβ species and mediate peptide aggregation have been constructed.[20-22] Small molecules, exhibited to specifically modify the aggregation of metal–Aβ over metal-free Aβ, have also been invented.[23-25] In addition, several antioxidants have been shown as chemical tools against ROS-induced oxidative stress.[26,27] Moreover, given that the individual elements have been detected to be intertwined with each other in the AD-affected brain, the design of small molecules as multifunctional tools for regulating the inter-connections among AD pathogenic components has currently received attention.[28-39] For example, some small molecules, including (*E*)-5-(4-hydroxystyryl)quinolone-8-ol (**10c**),[32] *N*,*N*-dimethyl-*p*-phenylenediamine (**DMPD**),[37] and N^1-((1*H*-pyrrol-2-yl)methyl)-N^4,N^4-dimethylbenzene-1,4-diamine (**4**),[39] were shown to alter the aggregation of metal-free Aβ and metal–Aβ as well as quench free radicals. Taken together, the efforts on engineering chemical tools able to target and control single or multiple pathogenic components(s) and control their activities have been made to provide molecular-level insights into the pathology of AD. The development of such tools, however, has been challenging.

Herein, we report new small molecules (**1**–**3**; Figure 2.1) that distinguishably interact and react with the pathological targets found in AD (*i.e.*, metal-free Aβ, metal–Aβ, and free radicals). Our compounds, **1**–**3**, were designed *via* a rational structure-property-directed strategy. As depicted in Figure 2.1, through an extremely minor structural variation [*i.e.*, change of only one nitrogen (N) or sulfur (S) donor atom in the backbone], we are able to tune the properties of compounds (*e.g.*, oxidation potentials, interactions with metal-free and metal-bound Aβ) and subsequently afford reactivities against disparate pathological features. Overall, our studies demonstrate that small molecules as chemical tools for modulating distinct pathological components of AD can be rationally

ULSAN NATIONAL INSTITUTE OF SCIENCE AND TECHNOLOGY

constructed through a structure-property-based design strategy. Such design tactics would be further applied for devising chemical reagents utilized for other neurodegenerative disorders.

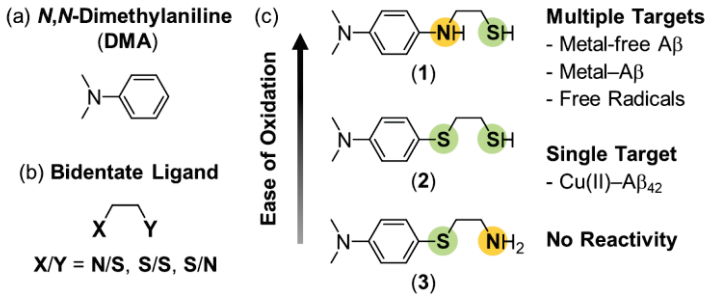

Figure 2.1. Rational design of the small molecules (**1**–**3**) able to have distinct properties and reactivities with pathological factors found in AD. (a,b) Structures of **DMA** and the bidentate ligands used for construction of **1**–**3**. (c) Structural variations of **1**–**3**, obtained *via* a change of only one N or S donor atom in the framework, and the difference in their oxidation and targets.

2.2 Results and Discussion

2.2.1. Structure-Property-Directed Principle for Designing Chemical Tools Able to Target Distinct Pathological Components of AD

To design the backbone of the new compounds (**1**–**3**), we rationally selected two structural moieties, *i.e.*, **DMA** and bidentate ligands composed of N and S donor atoms (Figure 2.1a,b). The conjugation of two structural groups could achieve different redox properties of small molecules and their distinguishable interactions with metal ions, metal-free Aβ, metal–Aβ, and free radicals. First, **DMA** (Figure 2.1a) is a structural portion employed for previously reported chemical tools targeting metal-free Aβ and/or metal–Aβ.[34,37,40,41] In addition, the **DMA**-containing structures [*e.g.*, **DMPD**,[37] **4**[39]], incorporated with one N donor atom at the *para* position of the *N*,*N*-dimethyl group, are known to undergo one- or two-electron oxidation.[37,39,42,43] Such oxidation is indicated to direct the capabilities of compounds against regulation of metal-free Aβ, metal–Aβ, and free radicals.[37,39,44] Second, in order to interact with metal ions [*i.e.*, Cu(II), Zn(II)] as well as metal ions bound to Aβ, the bidentate ligands containing N and S donor atoms were introduced into the framework of **1**–**3** (Figure 2.1b).[45,46] Lastly, to tune the extent of compounds' oxidation, **1**–**3** were obtained through the modification of only one N or S donor atom (Figure 2.1c). The oxidation potentials of small molecules have been previously demonstrated to be critical for interactions and reactivities with pathological targets, including metal-free Aβ, metal–Aβ, and free radicals.[39,44] As summarized in Figure 2.1c, our new molecules (**1**–**3**), developed *via* a very slight structural variation, are observed to have the differences in their oxidation and coverage of pathological targets for interactions and reactivities (*vide infra*).

ULSAN NATIONAL INSTITUTE OF SCIENCE AND TECHNOLOGY

2.2.2. Synthesis and Characterization of 1–3

As described in Scheme 2.1, new small molecules (**1**–**3**) were prepared. Compound **1** was afforded by ring opening of ethylene sulfide with **DMPD**. Compounds **2** and **3** were obtained through copper-catalyzed C–S bond formation between 4-iodo-aniline and the corresponding alkanethiols, followed by conversion of terminal groups into thiol (for **2**) or amino (for **3**) functionality. Synthesis of **1**–**3** was confirmed by spectroscopic and spectrometric methods (Figures 2.2-2.4). Moreover, our molecules were verified to interact with Cu(II) and Zn(II) (Figure 2.5) as we designed. Furthermore, **1**–**3** are suggested to be blood-brain barrier (BBB) permeable based on the calculated and experimentally obtained values (logBB > −1.0 and $-\log P_e < 5.4$; Table 2.1).

Scheme 2.1. Synthetic routes to 1–3.

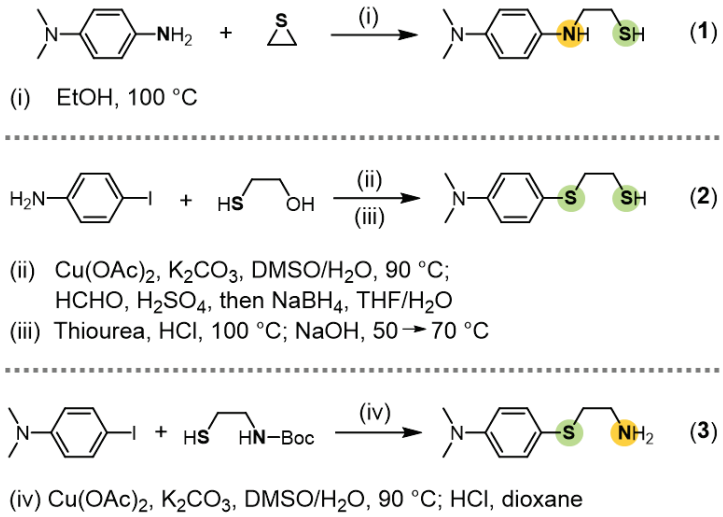

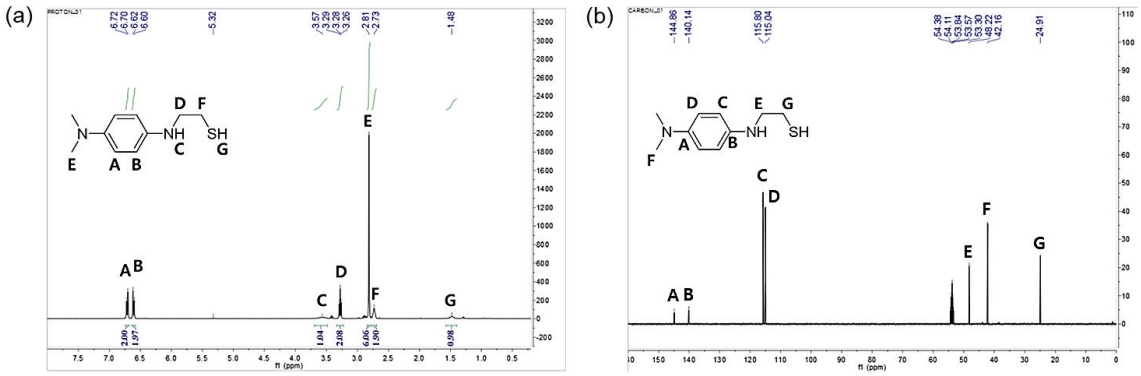

Figure 2.2. ^{1}H (a, 400 MHz) and ^{13}C (b, 100 MHz) NMR spectra of **1** in CD_2Cl_2.

ULSAN NATIONAL INSTITUTE OF SCIENCE AND TECHNOLOGY

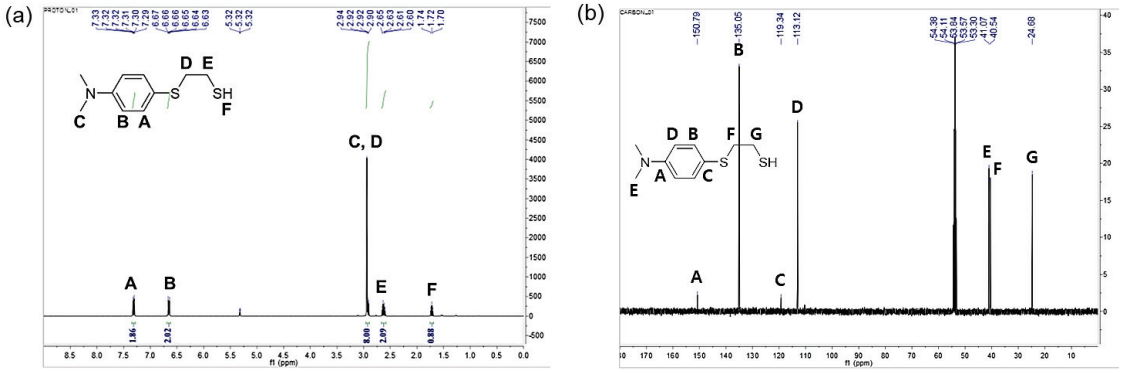

Figure 2.3. ^{1}H (a, 400 MHz) and ^{13}C (b, 100 MHz) NMR spectra of **2** in CD_2Cl_2.

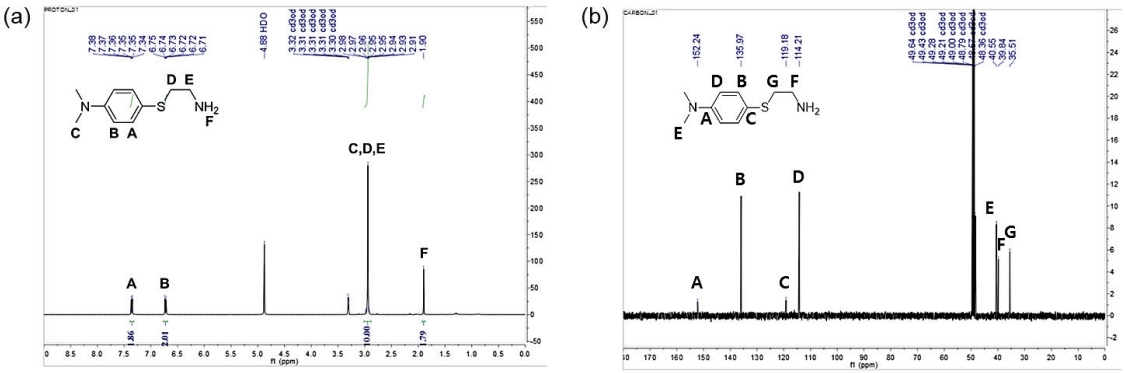

Figure 2.4. ^{1}H (a, 400 MHz) and ^{13}C (b, 100 MHz) NMR spectra of **3** in CD_3OD.

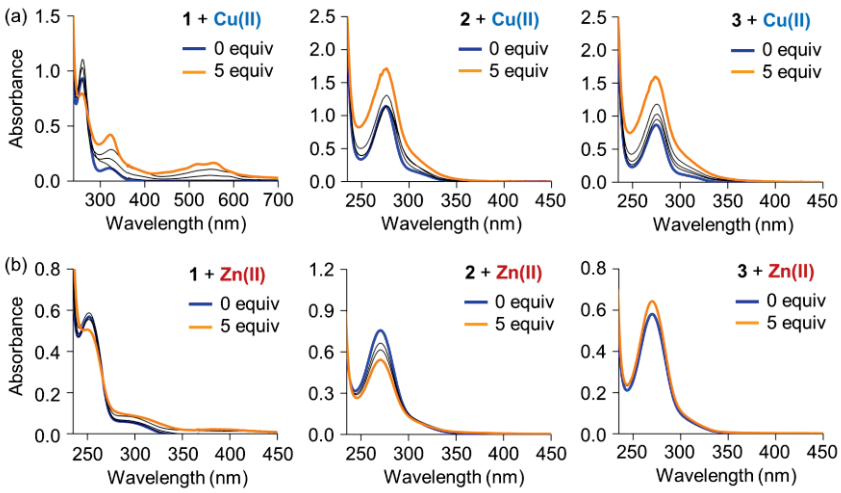

Figure 2.5. Metal binding of **1**–**3** observed by UV–Vis. Spectral changes of our molecules are monitored upon titration of various concentrations of (a) Cu(II) and (b) Zn(II). Conditions: [compound] = 50 μM, [$CuCl_2$ or $Zn(NO_3)_2$] = 0 (blue), 25, 50, 100, and 250 μM (orange), EtOH [for Cu(II) binding studies] or buffered solution [20 μM HEPES, pH 7.4, 150 μM NaCl, for Zn(II) binding studies], room temperature, incubation for 10 min.

ULSAN NATIONAL INSTITUTE OF SCIENCE AND TECHNOLOGY

Table 2.1. Values (MW, *c*log*P*, HBA, HBD, PSA, logBB, and –logP_e) of **1**–**3**.

	1	**2**	**3**	Lipinski's rules and others
MW[a]	196	213	196	≤ 450
*c*log*P*[b]	2.16	3.22	1.91	≤ 5.0
HBA[c]	2	1	2	≤ 10
HBD[d]	1	0	2	≤ 5
PSA (Å^2)[e]	15.3	3.24	29.3	≤ 90
logBB[f]	0.232	0.580	–0.0130	< –1.0 (poorly)
–logP_e[g]	4.59 ± 0.02 (CNS+)	4.52 ± 0.07 (CNS+)	4.45 ± 0.01 (CNS+)	–logP_e < 5.4 (CNS+) –logP_e > 5.7 (CNS–)

[a]MW, molecular weight, [b]*c*log*P*, calculated log of water-octanol partition coefficient, [c]HBA, hydrogen bond acceptor atoms, [d]HBD, hydrogen bond donor atoms, [e]PSA, polar surface area, [f]logBB = 0.152 × *c*log*P* − 0.0148 × PSA + 0.139, [g]–logP_e, the values obtained using the parallel artificial membrane permeability assay adapted for the BBB (PAMPA–BBB) were calculated by the PAMPA Explorer software v. 3.5. Compounds assigned to be CNS+ are able to penetrate the BBB and thus be available in the central nervous system (CNS), compounds assigned to be CNS– compounds have poor BBB permeability and thus their availability in the CNS are considered minimal.

2.2.3. Redox Properties of 1–3

To determine whether a minor structural variation of compounds could lead to distinguishable compounds' oxidation potentials as we designed (Figure 2.1), their redox properties were investigated by cyclic voltammetry (CV) and UV–visible spectroscopy (UV–Vis). The oxidation potentials of each compound were measured by CV (Figures 2.6 and 2.7). The lower value of the anodic peak potential (E_{pa}) indicates that the compound is relatively easy to be oxidized.[47] The E_{pa} value of **1** containing a moiety of **DMPD** is *ca.* 0.22 V [*versus* Ag/Ag(I)], significantly lower than those of **2** and **3** (E_{pa} = *ca.* 0.54/0.80 and 0.75 V, respectively) composed of a 4-(dimethylamino)-benzenethiol (**BT**) group (Figure 2.6 and Table 2.2). Although the E_{pa} values of **2** and **BT** could not be measured in H_2O due to their limited solubility, **1** has a much lower E_{pa} value than **3** in H_2O, similar to the observation in DMSO (Figure 2.7 and Table 2.3). Based on the E_{pa} values of **DMPD** and **BT** (*ca.* 0.23 and 0.93 V, respectively), the structural portion of **DMPD** would be mainly responsible for the lower E_{pa} value of **1**.

ULSAN NATIONAL INSTITUTE OF SCIENCE AND TECHNOLOGY

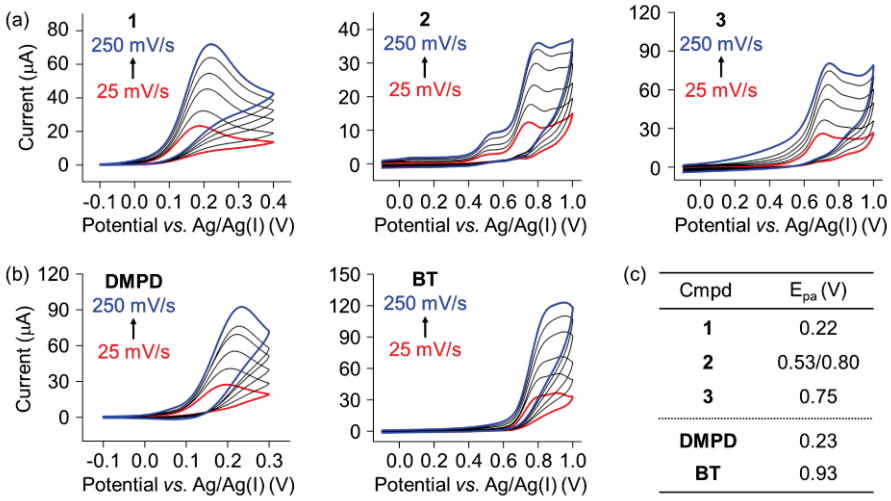

Cmpd	E_{pa} (V)
1	0.22
2	0.53/0.80
3	0.75
DMPD	0.23
BT	0.93

Figure 2.6. Redox potentials of **1**–**3** measured in DMSO. The oxidation of (a) **1**–**3** and (b) their structural portions was monitored by cyclic voltammetry. The E_{pa} values at 250 mV/s are summarized in (c). Conditions: [compound] = 1 mM; 0.1 M *tetra-N*-butylammonium perchlorate (in DMSO); various scan rates [25 (red), 50, 100, 150, 200, and 250 mV/s (blue)]; room temperature; three electrodes composed of the glassy carbon working electrode, platinum counter electrode, and Ag/Ag(I) reference electrode.

Table 2.2. Quantitative data of cyclic voltammograms of **1**–**3** in DMSO.

Scan rate (mV/s)	**1**		**2**			
	E_{pa} (V)	E_{pa} (V)	E_{pa} (V)	i_{pa} (μA)	E_{pa} (V)	i_{pa} (μA)
25	0.186	0.186	0.520	1.25	0.750	6.67
50	0.196	0.196	0.522	2.39	0.756	9.69
100	0.208	0.208	0.532	2.82	0.779	12.2
150	0.214	0.214	0.534	3.66	0.784	14.4
200	0.219	0.219	0.538	4.40	0.796	15.1
250	0.220	0.220	0.538	4.41	0.802	17.5
Scan rate (mV/s)	**3**		**DMPD**		**BT**	
	$E_{pa,1}$ (V)	$i_{pa,1}$ (μA)	$E_{pa,2}$ (V)	$i_{pa,2}$ (μA)	E_{pa} (V)	i_{pa} (μA)
25	0.704	16.8	0.191	17.0	0.919	25.2
50	0.719	23.5	0.204	25.2	0.919	39.9
100	0.732	31.7	0.218	34.8	0.933	46.2
150	0.734	38.1	0.224	40.8	0.938	66.6
200	0.748	41.1	0.226	40.9	0.938	80.8
250	0.747	37.8	0.232	49.4	0.933	83.6

ULSAN NATIONAL INSTITUTE OF SCIENCE AND TECHNOLOGY

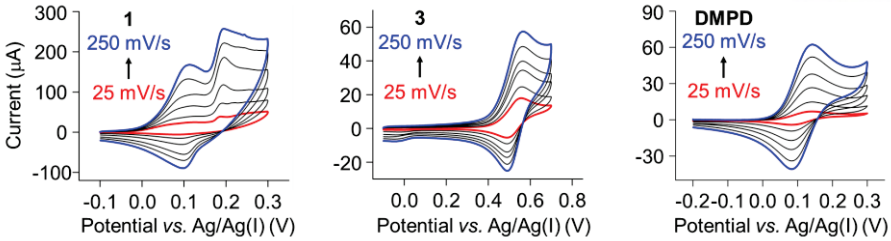

Figure 2.7. Redox potentials of **1**–**3** measured in H_2O. The oxidation of **1**, **3**, and **DMPD** was monitored by cyclic voltammetry. Conditions: [compound] = 1 mM, 1 M NaCl (in ddH_2O), various scan rates [25 (red), 50, 100, 150, 200, and 250 mV/s (blue)], room temperature, three electrodes composed of the glassy carbon working electrode, platinum counter electrode, and Ag/Ag(I) reference electrode.

Table 2.3. Quantitative data of cyclic voltammograms of **1**–**3** in H_2O.

Scan rate (mV/s)	**DMPD**			
	E_{pa} (V)	i_{pa} (μA)	E_{pc} (V)	i_{pc} (μA)
25	0.138	4.19	0.0830	4.16
50	0.141	8.88	0.0840	8.68
100	0.139	14.8	0.0820	14.1
150	0.140	22.9	0.0840	22.5
200	0.140	31.8	0.0840	26.4
250	0.141	37.6	0.0860	34.2
Scan rate (mV/s)	**1**			
	E_{pa} (V)	i_{pa} (μA)	E_{pc} (V)	i_{pc} (μA)
25	0.0960	8.91	–	–
50	0.107	12.4	0.0994	1.90
100	0.111	25.6	0.0987	3.67
150	0.103	22.7	0.103	5.94
200	0.106	44.4	0.101	11.3
250	0.109	58.0	0.100	15.8
Scan rate (mV/s)	**3**			
	E_{pa} (V)	i_{pa} (μA)	E_{pc} (V)	i_{pc} (μA)
25	0.557	10.4	0.491	5.00
50	0.560	13.8	0.488	6.63
100	0.560	17.4	0.491	8.11
150	0.563	19.9	0.490	8.24
200	0.565	23.5	0.488	12.5
250	0.567	28.7	0.491	17.2

In addition to the moieties of **DMPD** and **BT**, the oxidation of the thiol groups in **1** and **2** was monitored by the DTNB assay [DTNB = 5,5'-dithio-*bis*-(2-nitrobenzoic acid)] with *L*-cysteine as a positive control (Scheme 2.2 and Figure 2.8). A new absorption band at *ca.* 412 nm was exhibited

ULSAN NATIONAL INSTITUTE OF SCIENCE AND TECHNOLOGY

upon reaction of the thiol groups in **1** and **2** with the disulfide bond in DTNB, indicative of the formation of 2-nitro-5-thiobenzoic acid dianion (TNB^{2-}) (Figure 2.8). The different intensity of the optical bands of TNB^{2-}, resulted from the interactions of DTNB with compounds, presents that the thiol group in **1** is less oxidizable than that in **2**.

Scheme 2.2. Reaction scheme of the DTNB assay

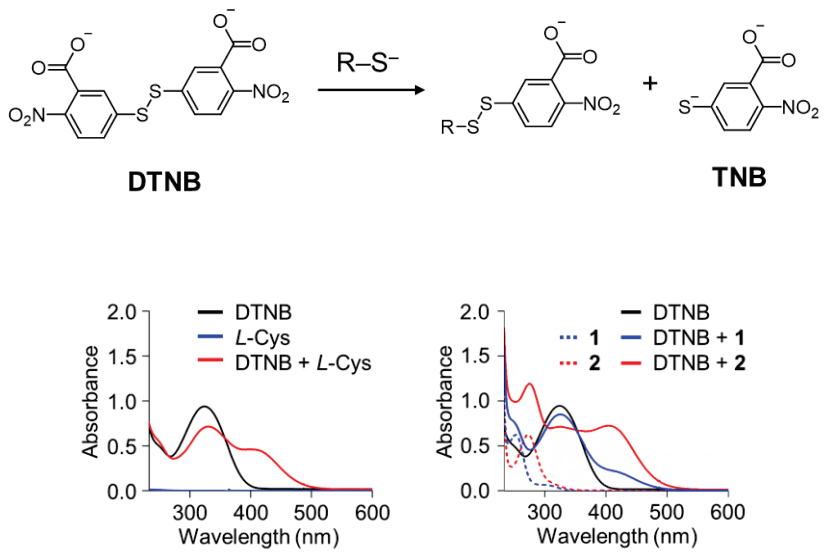

Figure 2.8. Oxidation of thiol groups in *L*-cysteine (*L*-Cys) and compounds, monitored by the DTNB assay. *L*-Cys was used as a positive control in the DTNB assay. Conditions: [DTNB] = 50 μM; [compound] = 50 μM; buffered solution (pH 8.0); room temperature; incubation for 10 min.

Based on the redox properties of **1**–**3**, analyzed through CV and the DTNB assay, their oxidation was additionally traced for 24 h by UV–Vis (Figure 2.9). The absorption band of **1** decreased at *ca.* 254 nm and increased at *ca.* 300 nm upon incubation, indicative of oxidation producing the delocalized electron(s) on the phenyl ring.[37,39] Different from **1**, the intensity of the optical band of **2** was slightly reduced at *ca.* 280 nm, whereas the peak intensity was enhanced in the range of *ca.* 290 to 400 nm. The spectral changes of **3** were not detected even for 24 h (Figure 2.9), suggesting that the compound was not easily oxidizable under our experimental conditions. Therefore, the moiety of **DMPD** in **1** is suggested to be more associated with ligand oxidation than the **BT** portion found in **2** and **3**, which is consistent with the results of CV (Figure 2.6). More importantly, the different degree of the compounds' oxidation is demonstrated to be achieved *via* a minor structural difference (*i.e.*, replacement of only one donor atom in the backbone; Figure 2.1c). These distinct redox properties of compounds are observed to direct their distinguishable interactions as well as modulating reactivities towards metal-free Aβ, metal–Aβ, and free radicals (*vide infra*).

ULSAN NATIONAL INSTITUTE OF SCIENCE AND TECHNOLOGY

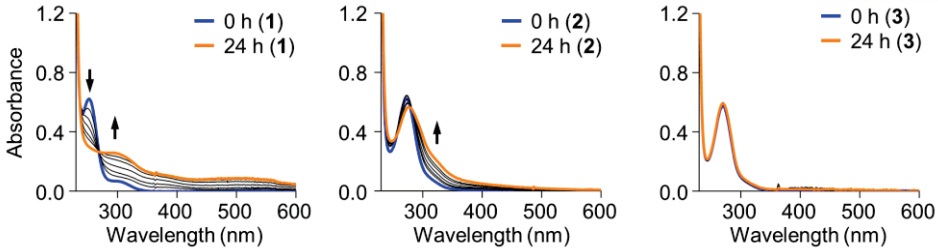

Figure 2.9. Oxidation of **1**–**3** monitored by UV–Vis. Conditions: [compound] = 50 μM; 20 μM HEPES, pH 7.4, 150 μM NaCl; room temperature; incubation for 24 h.

2.2.4. Interactions of 1–3 with Metal-free Aβ

To verify how the distinct redox properties of **1**–**3** could influence their reactivities towards Aβ aggregation, the interactions of **1**–**3** with metal-free Aβ species were identified at the molecular level employing electrospray ionization mass spectrometry (ESI–MS) and tandem MS (ESI–MS^2) (Figure 2.10). Upon incubation of metal-free $A\beta_{40}$ with or without the compounds, the +3-charged $A\beta_{40}$ monomer ($[A\beta_{40} + 3H]^{3+}$) was detected at 1444 *m/z* in the ESI–MS spectra (red peaks; Figure 2.10a). Among our small molecules, **1** was observed to oxidize metal-free $A\beta_{40}$ showing the peak at 1449 *m/z* corresponding to $[A\beta_{40} + O + 3H]^{3+}$ (red asterisk; Figure 2.10a), while such peptide modification was not monitored in the case of metal-free $A\beta_{40}$ treated with both **2** and **3**.

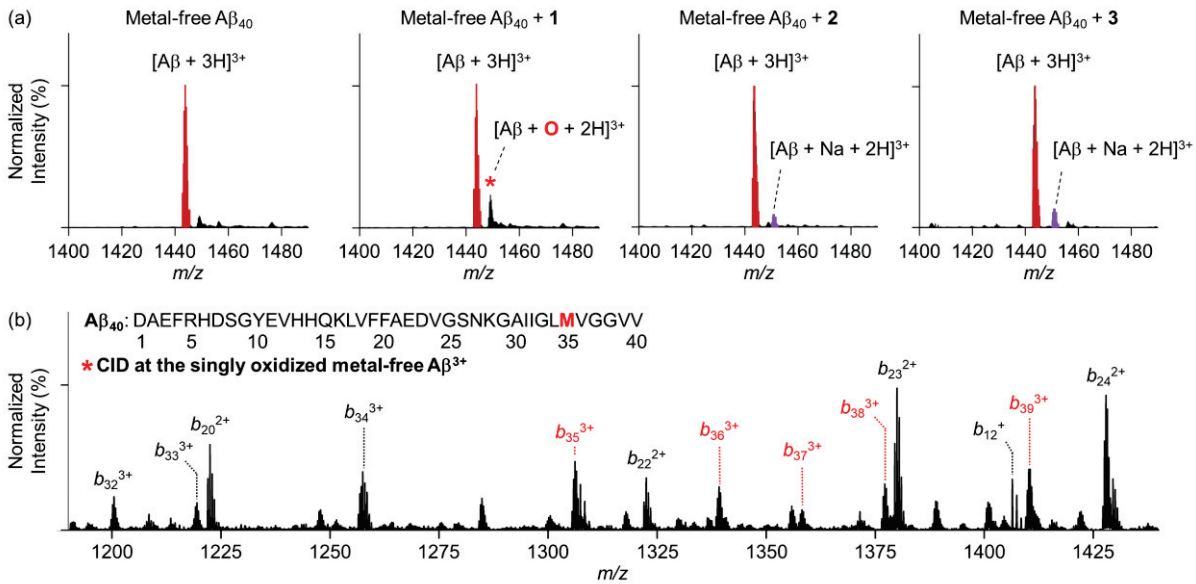

Figure 2.10. Interactions of **1**–**3** with metal-free $A\beta_{40}$, analyzed by ESI–MS and ESI–MS^2. (a) The +3-charged $A\beta_{40}$ monomers in the samples incubated with **1**–**3** in the absence of Cu(II) were detected in the ESI–MS spectra. Metal-free $A\beta_{40}$ is denoted as red peaks. The oxidized ions are indicated by the red asterisks. (b) The oxidized amino acid residue of $A\beta_{40}$ incubated with **1** was identified through

ULSAN NATIONAL INSTITUTE OF SCIENCE AND TECHNOLOGY

ESI–MS^2. Conditions: [Aβ_{40}] = 100 μM; [compound] = 500 μM; incubation for 3 h; 20 mM ammonium acetate, pH 7.2; 37 °C; no agitation. All samples were diluted with ddH_2O by 10 fold before injection to the mass spectrometer.

Furthermore, we determined which amino acid residues of metal-free Aβ_{40} were plausibly oxidized upon treatment of **1** through ESI–MS^2 (Figure 2.10b). The ESI–MS^2 spectrum of **1**-added Aβ_{40} displayed that the methionine 35 (M35) residue in Aβ_{40} was oxidized (*e.g.*, methionine sulfoxide).[48,49] In the previous studies, the oxidation of M35 in Aβ has been suggested to modify Aβ aggregation pathways.[50,51] Together, among our molecules (**1**–**3**), **1** with the lowest E_{pa} value is capable of oxidizing metal-free Aβ_{40}, implying that the interactions of compounds with metal-free Aβ_{40} could be linked to their redox properties.

2.2.5. Interactions of 1–3 with Cu(II)–Aβ

In addition to metal-free Aβ_{40}, the interactions of **1**–**3** with Cu(II)-treated Aβ_{40} species were investigated (Figure 2.11). Note that compounds' interactions with Zn(II)–Aβ could not be studied since Zn(II)- bound Aβ species were not observed under our MS conditions. Upon incubation of Aβ_{40} in the presence of Cu(II), Cu(II)- added Aβ_{40} (*i.e.*, [Aβ_{40} + Cu(II) + H]$^{3+}$) was revealed at 1465 *m/z*, along with metal-free Aβ_{40} at 1444 *m/z* (red and light blue peaks; Figure 2.11). Compound **1** with the lowest oxidation potential was shown to degrade and oxidize Cu(II)-treated Aβ_{40} (orange peaks and red asterisks, respectively; Figure 2.11). The degraded Aβ_{40} by 89 Da could be induced by oxidative cleavage of the aspartate 1 (D1) residue forming isocyanate.[52-54] The D1 residue was reported to be preferentially oxidized through alkoxyl radical pathways,[52-54] which could impact the structural rearrangement of Cu(II) coordination in Aβ. In addition to the degraded Aβ_{40} (at 1415 *m/z*), the peak at 1409 *m/z* could be assigned as the degraded Aβ_{40} with further loss of one water (H_2O) molecule. In a similar manner, the peaks at 1421 *m/z* and 1427 *m/z* (peptide species bound to one and two H_2O, respectively) might indicate the degradation of Aβ_{40}.

The oxidation sites in the amino acid sequence of Cu(II)-added Aβ_{40} induced by **1** were determined by ESI–MS^2 (Figure 2.11b). Under Cu(II)-present conditions, histidine 13 and 14 (H13 and H14) were shown to be oxidized, along with M35, previously reported as the plausibly oxidizable residues in Aβ.[48,50,51,55,56] Since Cu(II) is known to be bound to H13 and H14 in Aβ,[3,5,45] their oxidation (*e.g.*, 2-oxo histidine)[57] upon incubation of Aβ with **1** might explain the low abundance of Cu(II)–Aβ_{40} in the spectra (Figure 2.11b). Additionally, the oxidation of H13, H14, and M35 in Aβ is previously reported to alter Aβ aggregation pathways.[50,51]

ULSAN NATIONAL INSTITUTE OF SCIENCE AND TECHNOLOGY

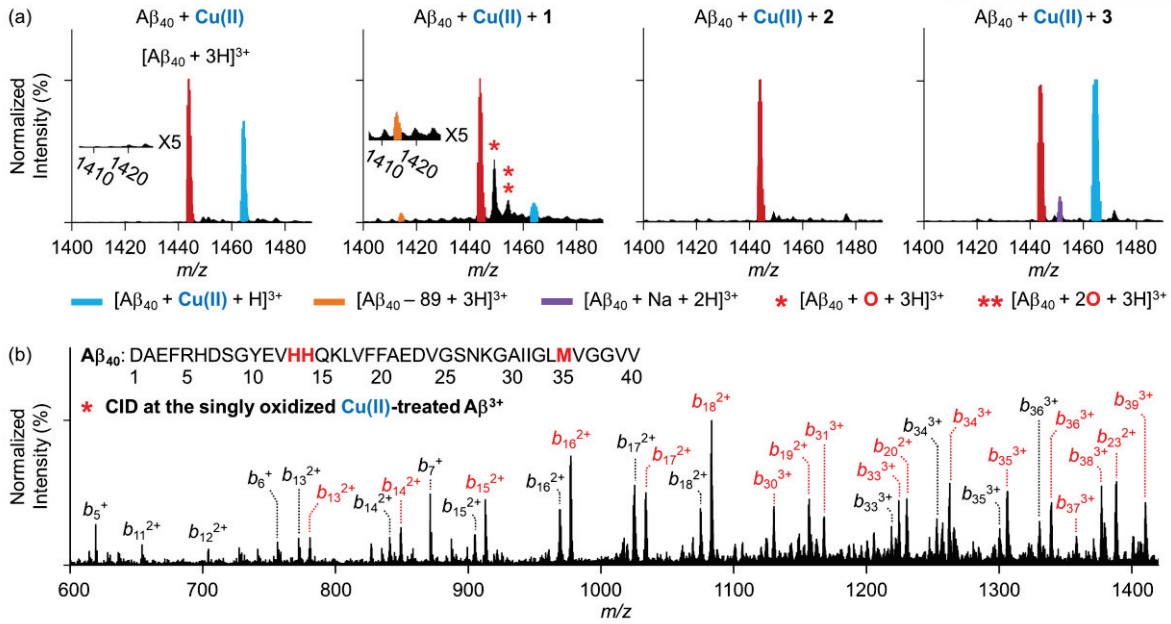

Figure 2.11. Interactions of **1**–**3** with Cu(II)-treated $A\beta_{40}$, analyzed by ESI–MS and ESI–MS^2. (a) The +3-charged $A\beta_{40}$ monomers in the samples incubated with **1**–**3** in the presence of Cu(II) were detected in the ESI–MS spectra. Cu(II)–$A\beta_{40}$ is denoted as light blue peaks, respectively. The oxidized ions are indicated by the red asterisks. The number of the asterisks represents the number of the oxygen atoms incorporated into $A\beta_{40}$. The degraded $A\beta_{40}$ with 89 Da loss (orange peaks) was presented from the **1**-treated samples in the presence of Cu(II). (b) The oxidized amino acid residues of $A\beta_{40}$ incubated with **1** and Cu(II) were identified through ESI–MS^2. Conditions: [$A\beta_{40}$] = 100 μM; [$CuCl_2$] = 100 μM; [compound] = 500 μM; incubation for 1 h; 20 mM ammonium acetate, pH 7.2; 37 °C; no agitation. All samples were diluted with ddH_2O by 10 fold before injection to the mass spectrometer.

Compound **2**, which possesses the higher oxidation potential than **1** (Figure 2.6), indicated different interactions with Cu(II)-treated $A\beta_{40}$, compared with **1**. In detail, **2** significantly reduced the intensity of peaks at 1465 *m/z* corresponding to [$A\beta_{40}$ + Cu(II) + H]$^{3+}$, suggesting that the coordination of Cu(II) to $A\beta_{40}$ was modified by incubation with **2** (Figure 2.11). Distinct from **1**, **2** was not able to degrade and oxidize Aβ even in the presence of Cu(II). In order to further analyze the interaction of **2** with Cu(II)–Aβ, we additionally employed Cu(II)-treated $A\beta_{42}$, another isoform of Aβ (Figure 2.12).[12] When **2** was incubated with Cu(II) and $A\beta_{42}$, the peak of Cu(II)–$A\beta_{42}$ disappeared, supporting that this molecule might also disrupt Cu(II) binding to $A\beta_{42}$ (blue peaks; Figure 2.12a). Moreover, compound **2** was observed to be transformed to **BT**[58] (153 Da) or the oxidized **BT** (**BT_{ox}**; 304 Da) under Cu(II)-present conditions. These transformed compounds from **2**, **BT** and **BT_{ox}**, were shown to subsequently form the non-covalent adduct with the $A\beta_{42}$ dimer at 1868 *m/z* (green peaks; Figure 2.12a). Moving forward, we applied ion mobility mass spectrometry (IM–MS) to monitor the effects of **2** on conformation of the $A\beta_{42}$ dimer (Figure 2.12b). The arrival time distribution (ATD) of

ULSAN NATIONAL INSTITUTE OF SCIENCE AND TECHNOLOGY

the $A\beta_{42}$ dimer, monitored after addition of **2** into the sample of Cu(II)-treated $A\beta_{42}$, was enhanced at 11.57 ms, implying that **2** could trigger the conformational compaction of the dimeric form. Thus, **2** is able to specifically interact with Cu(II)-treated Aβ over metal-free Aβ, especially showing the non-covalent complexation between the compound and the $A\beta_{42}$ dimer with conformational changes when Cu(II) is present. These interactions of **2** with Cu(II)–$A\beta_{42}$ are exhibited to be related to its modulating activity towards the aggregation of Cu(II)–$A\beta_{42}$ (*vide infra*).

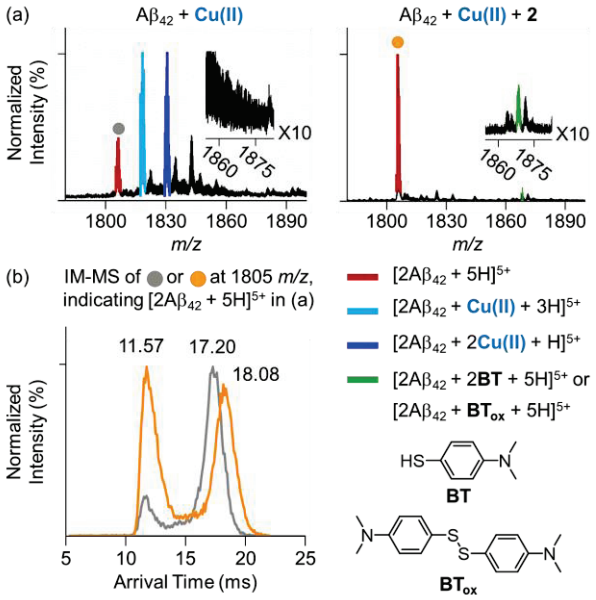

Figure 2.12. Interactions of **2** with Cu(II)-treated monitored $A\beta_{42}$ monitored by ESI–MS and IM–MS. (a) The +5-charged Cu(II)-treated $A\beta_{42}$ dimer in the samples incubated without (left) or with **2** (right). The non-covalent complex formation of **BT** (153 *m/z*) or $\mathbf{BT_{ox}}$ (304 *m/z*) with $A\beta_{42}$ was detected in the ESI–MS spectra (green peak, 1868 *m/z*). (b) The altered arrival time distributions (ATDs) of Cu(II)–$A\beta_{42}$ upon incubation with **2** indicate the conformational change of the peptide. Ions selected for the IM–MS analysis are marked with gray and orange circles in the ESI–MS spectra. Conditions: [$A\beta_{42}$] = 100 μM; [$CuCl_2$] = 100 μM; [**2**] = 500 μM; incubation for 1 h; 20 mM ammonium acetate, pH 7.2; 37 °C; no agitation. All samples were diluted with ddH_2O by 10 fold before injection to the mass spectrometer.

Lastly, the hardly oxidizable compound **3**, relative to **1** and **2**, displayed no significant interaction with Cu(II)-treated $A\beta_{40}$. For example, **3** was not able to degrade and oxidize Aβ as well as generate non-covalent complexes with peptides (Figure 2.11b). In summary, the easily oxidized compound, **1**, is observed to considerably interact with both metal-free and Cu(II)-treated Aβ. Compound **2** (with the higher E_{pa} value than **1**) specifically affects Cu(II) binding to both $A\beta_{40}$ and $A\beta_{42}$ and produces a non-covalent adduct with the $A\beta_{42}$ dimer showing structural compaction. The least oxidizable compound, **3**, among our molecules could not interact with both metal-free Aβ and Cu(II)–Aβ. Taken

ULSAN NATIONAL INSTITUTE OF SCIENCE AND TECHNOLOGY

together, our MS studies support that the interactions between our compounds and metal-free or Cu(II)-treated Aβ could be differentiated depending on their redox properties which were rationally tuned *via* a very minor structural variation (Figure 2.1c).

2.2.6. Regulatory Abilities of 1–3 against Metal-free Aβ and Metal–Aβ Aggregation

To confirm the compounds' regulatory activities against metal-free Aβ and metal–Aβ, the capability of **1**–**3** to control peptide aggregation with and without metal ions was evaluated. The resultant Aβ species upon treatment with compounds were analyzed by gel electrophoresis/Western blotting (gel/Western blot; for size distribution) with an anti-Aβ antibody (6E10) and transmission electron microscopy (TEM; for morphology). In the inhibition experiments (Figure 2.13), freshly prepared Aβ was introduced with our compounds in the absence and presence of metal ions [*i.e.*, Cu(II) and Zn(II)] for 24 h. In the disaggregation experiments (Figure 2.14), the compounds were added to preformed metal-free or metal-added Aβ aggregates, generated by 24 h incubation, and the resultant samples were additionally incubated for 24 h. The larger Aβ aggregates (*e.g.*, fibrils), generated from both experiments, are known to limit their penetration through the gel matrix; thus, they are in general visualized by TEM.[59,60] When Aβ aggregation is varied with the treatment of compounds producing small-sized Aβ species, smearing bands in the gel/Western blot are presented.[59,60]

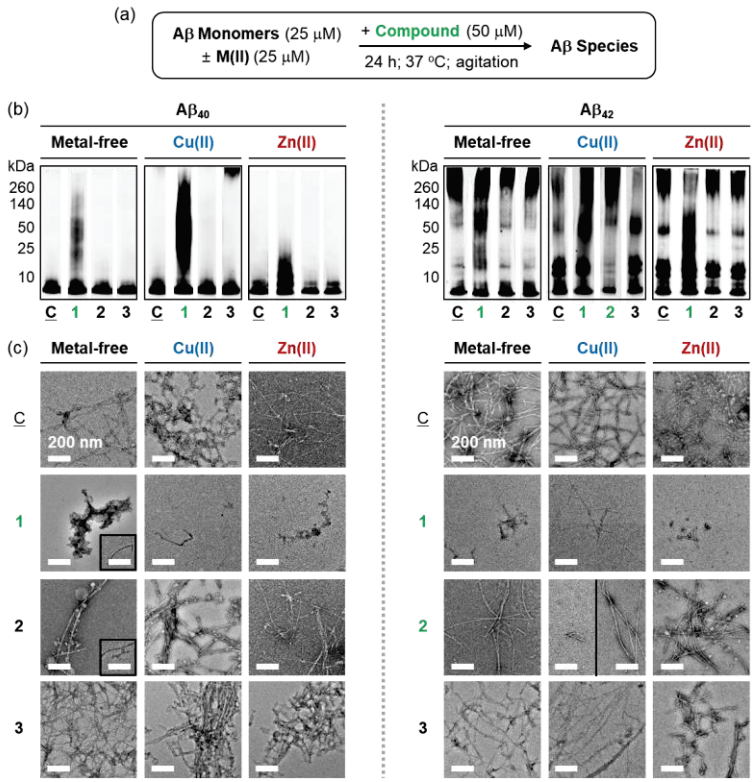

ULSAN NATIONAL INSTITUTE OF SCIENCE AND TECHNOLOGY

Figure 2.13. Reactivities of **1**–**3** to inhibit metal-free Aβ and metal–Aβ aggregation. (a) Scheme of the inhibition experiments. (b) Analysis of the size distributions of the resultant $A\beta_{40}$ and $A\beta_{42}$ species from (a) by gel/Western blot using 6E10. (**C**) [Aβ ± Cu(II) or Zn(II)]; (**1**) [(C) + **1**]; (**2**) [(C) + **2**]; (**3**) [(C) + **3**]. Conditions: [Aβ] = 25 μM; [$CuCl_2$ or $ZnCl_2$] = 25 μM; [compound] = 50 μM; pH 6.6 [for Cu(II) samples] or pH 7.4 [for metal-free and Zn(II) samples]; 37 °C; constant agitation. (c) TEM images of the samples from (b). The inset image represents the minor species. Scale bar = 200 nm.

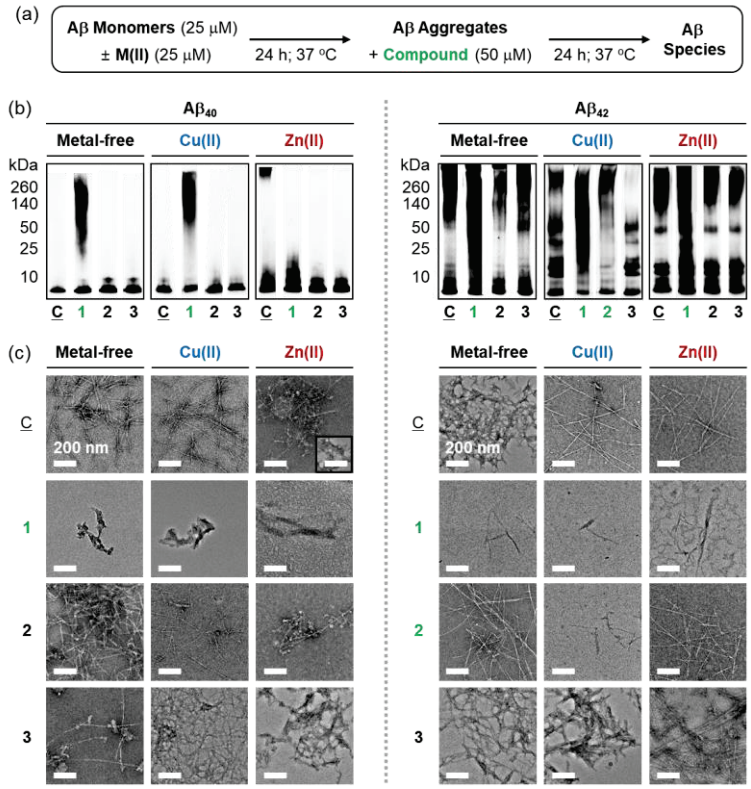

Figure 2.14. Reactivities of **1**–**3** against the preformed metal-free and metal-induced $A\beta_{40}/A\beta_{42}$ aggregates. (a) Scheme of the disaggregation experiments. (b) Analysis of the size distributions of the resultant $A\beta_{40}$ and $A\beta_{42}$ species from (a) by gel/Western blot using 6E10. (**C**) [Aβ ± Cu(II) or Zn(II)]; (**1**) [(C) + **1**]; (**2**) [(C) + **2**]; (**3**) [(C) + **3**]. Conditions: [Aβ] = 25 μM; [$CuCl_2$ or $ZnCl_2$] = 25 μM; [compound] = 50 μM; pH 6.6 [for Cu(II) samples] or pH 7.4 [for metal-free and Zn(II) samples]; 37 °C; constant agitation. (c) TEM images of the resultant $A\beta_{40}/A\beta_{42}$ aggregates from the 24 h incubated samples from (b). Scale bar = 200 nm.

When metal-free $A\beta_{40}/A\beta_{42}$ and metal–$A\beta_{40}/A\beta_{42}$ were incubated with **1**, noticeable smearing bands of the resultant $A\beta_{40}$ and $A\beta_{42}$ species with lower molecular weights were observed in the gel/Western blots (Figure 2.13b). These results suggest that **1** is able to significantly modulate Aβ aggregation pathways in the absence and presence of metal ions. In addition, **1** is shown to disaggregate preformed metal-free $A\beta_{40}/A\beta_{42}$ and metal–$A\beta_{40}/A\beta_{42}$ aggregates or affect their further

ULSAN NATIONAL INSTITUTE OF SCIENCE AND TECHNOLOGY

aggregation (Figure 2.14b). TEM images of the Aβ aggregates formed upon treatment of **1** in both inhibition and disaggregation studies were amorphous and smaller sized instead of larger and fibrillar aggregates observed from compound-free Aβ samples (Figures 2.13c and 2.14c).

In the case of **2**, this molecule could not regulate metal-free $A\beta_{40}$ and metal–$A\beta_{40}$ aggregation in both inhibition and disaggregation experiments (Figures 2.13b and 2.14b). Different from $A\beta_{40}$, smearing bands of Cu(II)–$A\beta_{42}$ aggregates, larger than 140 kDa, were observed upon incubation with **2**, which could indicate its specific reactivity towards the aggregation of Cu(II)–$A\beta_{42}$ over metal-free $A\beta_{42}$ and Zn(II)–$A\beta_{42}$ (Figures 2.13b and 2.14b). In accordance with the results of gel/Western blot, shorter-sized Aβ aggregates were shown only in the samples containing **2** and Cu(II)-treated $A\beta_{42}$ in both inhibition and disaggregation experiments (Figures 2.13c and 2.14c). Lastly, **3** could not modify the aggregation of metal-free $A\beta_{40}$/$A\beta_{42}$ and metal–$A\beta_{40}$/$A\beta_{42}$ based on the results of gel/Western blot (Figures 2.13b and 2.14b). No noticeable morphological changes of **3**-added Aβ aggregates, produced with and without metal ions, were visualized (Figures 2.13c and 2.14c).

The reactivities of **1**–**3** against the aggregation of metal-free Aβ and metal–Aβ are consistent with the trend of their E_{pa} values (Figure 2.6) as well as the observation for the interactions with metal-free and metal-bound Aβ species (Figures 2.10-2.12). Compound **1** with the lowest E_{pa} value could trigger the oxidation of metal-free Aβ (at M35) as well as the degradation (at D1) and oxidation (at H13, H14, and M35) of Cu(II)–Aβ. Such interactions could lead to modifying metal-free and metal-induced Aβ aggregation by **1**. Compound **2** with the higher E_{pa} value than **1** could disrupt the coordination of Cu(II) to Aβ and generate a non-covalent complex with the $A\beta_{42}$ dimer showing structural compaction with Cu(II) being present; thus, the molecule could noticeably control Cu(II)–$A\beta_{42}$ aggregation. In the case of **3** with the highest E_{pa} value among our molecules, the compound was not able to interact with metal-free Aβ and Cu(II)–Aβ, which could support no reactivities of the molecule towards the aggregation of both metal-free Aβ and metal–Aβ. Taken together, the ability of compounds to modulate the aggregation of $A\beta_{40}$ and $A\beta_{42}$ with or without metal ions is demonstrated to be highly relevant to their characteristics, including redox properties and interactions with the targets.

2.2.7. Antioxidant Capabilities of 1–3 against Free Radicals

To determine if the redox properties of compounds can direct their regulatory activity against free radicals, the ability of **1**–**3** to quench free radicals was evaluated by the Trolox equivalent antioxidant capacity (TEAC) assay employing the lysates of Neuro-2a (N2a) neuroblastoma cells (Figure 2.15a). The TEAC assay verifies the capability of compounds to scavenge free radicals, such as $ABTS^{+\bullet}$ [ABTS = 2,2'-azino*bis*-(3-ethylbenzothiazoline-6-sulfonic acid)], relative to that of an analog of vitamin E, Trolox (6-hydroxy-2,5,7,8-tetramethylchroman-2-carboxylic acid).[39,61-63] The quenching

ULSAN NATIONAL INSTITUTE OF SCIENCE AND TECHNOLOGY

ability of Trolox against free radicals is well characterized; thus, small molecules with the TEAC values higher than 1.0 are regarded as potent antioxidants than Trolox.[61] Compound **1** is presented to have the TEAC value as 1.6 (± 0.1), suggesting this molecule as a better scavenger against free radicals than Trolox (Figure 2.15). Compound **2** also quenches free radicals [the TEAC value as 0.33 (± 0.04)] but its activity is much lower than **1** and Trolox. As expected, **3** with the highest oxidation potential exhibits the lowest TEAC value [0.03 (± 0.01)]. Collectively, the trend of the TEAC values of **1**–**3** is observed to be well matched with the degree of their oxidation (Figures 2.6 and 2.7).

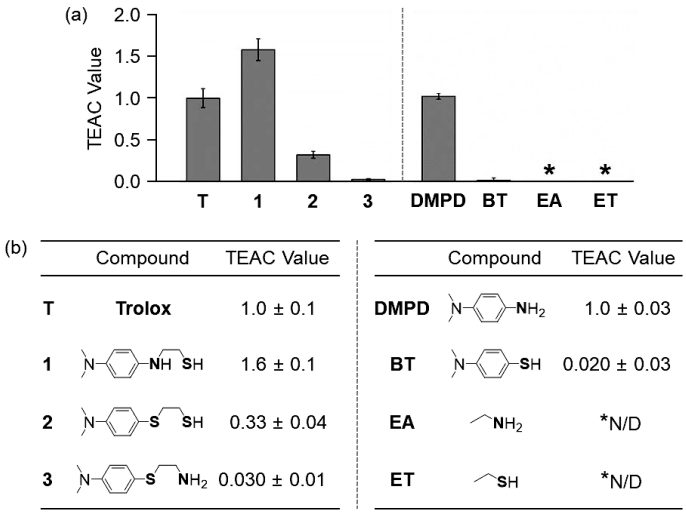

Figure 2.15. Scavenging capability of **1**–**3** against free organic radicals in N2a cell lysates, determined by the TEAC assay. The TEAC values of compounds are summarized in (b). *n.d., not determined. The TEAC values of ethanamine (**EA**) and ethanethiol (**ET**) were not able to be obtained due to their limited activity.

In order to identify which structural portions contribute to the antioxidant capability of our compounds (especially, **1** and **2**), we further investigated the ability of structural components of **1**–**3** [*i.e.*, **DMPD**, **BT**, ethanamine (**EA**), ethanethiol (**ET**); Figure 2.15] to scavenge free radicals. The TEAC value of **DMPD** is 1.0 (± 0.03), much higher than that of **BT** [0.02 (±0.03)], which could explain the better antioxidant capability of **1** containing **DMPD**, compared to **2** and **3** possessing **BT**. In the case of **EA** and **ET**, their TEAC values could not be measured due to their limited activity against free radicals. In addition to the individual parts, the entire structure of the compounds might be shown to be important for their antioxidant capacity (**1** *versus* **DMPD**; Figure 2.15b). Overall, the antioxidant capability of compounds is confirmed to be associated with their chemical structures that consequently differentiate their oxidation potentials.

ULSAN NATIONAL INSTITUTE OF SCIENCE AND TECHNOLOGY

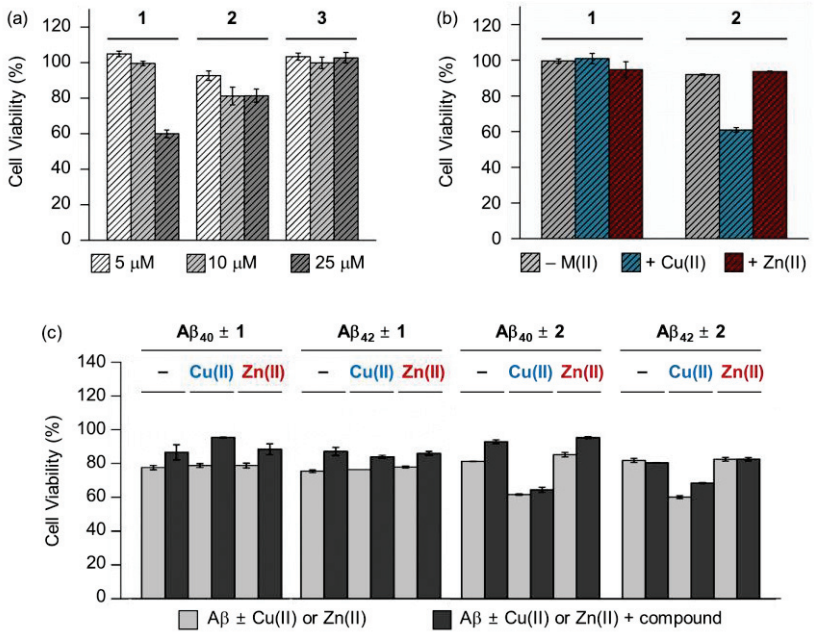

Figure 2.16. Toxicity of compounds in SH-SY5Y (5Y) cells. (a) Cell survival of compounds (**1**–**3**) in the absence of metal ions. (b) Cell survival of compounds (*i.e.,* **1** and **2**) in the presence of metal ions. (c) Cell survival of compounds (*i.e.,* **1** and **2**) in the presence of $A\beta_{40}$ or $A\beta_{42}$ and metal ions. Conditions: [Aβ] = 10 μM, [$CuCl_2$ or $ZnCl_2$] = 5 μM, [compound] = 10 μM.

2.3. Conclusions

Novel small molecules, composed of **DMA** and bidentate ligands, were newly constructed for regulating distinct factors linked to AD pathology to different extents. The development of such compounds was achieved *via* our rational structure-property-directed design principle employing a very straightforward structural modification. The distinguishable characteristics of the small molecules, including redox properties and interactions with pathological components, were obtained through our simple structural variation. The relatively easily oxidizable compound, **1**, is demonstrated to effectively modify multiple pathogenic factors, *i.e.*, metal-free and metal-bound Aβ as well as free radicals. In addition, **2**, which is less easily oxidized than **1**, presents the specific reactivity towards the aggregation of Cu(II)–$A\beta_{42}$, along with less scavenging ability against free radicals than that of **1**. The hardly oxidizable compound, **3**, could not influence the actions of all pathogenic components, *i.e.*, metal-free Aβ, metal–Aβ, and free radicals. Therefore, our studies reveal that a very minor structural change could successfully tune their properties (especially, oxidation potentials) as well as regulatory reactivities towards distinct pathogenic elements found in AD.

In order to evaluate biological applications of our small molecules, their cytotoxicity was examined employing human neuroblastoma SH-SY5Y cells through the MTT assay [MTT = 3-(4,5-dimethylthiazol-2-yl)-2,5-diphenyltetrazolium bromide] (Figure 2.16). Compound **1** was observed to have no cytotoxicity up to 10 μM (cell viability, *ca.* 100%; Figure 2.16). In the case of **2** and **3**, the

ULSAN NATIONAL INSTITUTE OF SCIENCE AND TECHNOLOGY

compounds were less toxic up to 25 μM (cell viability, *ca.* 80-100%) (Figure 2.16). When the cells incubated with Aβ and **1** (the compound with regulatory reactivities towards multiple pathological factors) in the absence and presence of metal ions, the cell survival was enhanced by *ca.* 10 to 20% (Figure 2.16). To improve the utilization of such molecules in biological systems, further structural optimization would be necessary. To conclude, our structure-property-directed design demonstrates the feasibility of building up novel structural entities useful for devising chemical tools towards modulation of single or multiple pathogenic factor(s) found in AD.

2.4. Experimental Section

2.4.1. Materials and Methods

All reagents were purchased from commercial suppliers and used as received unless otherwise noted. Cyclic voltammograms were recorded under N_2 (g) with a CHI620E model potentiostat (Qrins, Seoul, Republic of Korea). A three-electrode setup is composed of an Ag/Ag(I) reference electrode [RE-1B Reference electrode [Ag/Ag(I); Qrins], a Pt wire auxiliary electrode (SPTE Platinum electrode; Qrins), and a glassy carbon working electrode (Qrins). $A\beta_{40}$ and $A\beta_{42}$ ($A\beta_{42}$ = DAEFRHDSGYEVHHQKLVFFAEDVGSNKGAIIGLMVGGVVIA) were purchased from Anaspec (Fremont, CA, USA). Trace metal ions were removed from the solutions used in the studies by treating the solutions with Chelex overnight (Sigma-Aldrich, St. Louis, MO, USA). Optical spectra were recorded using an Agilent 8453 UV–Vis spectrophotometer. Absorbance values for biological assays, including the PAMPA–BBB, TEAC, and MTT assays, were measured using a Molecular Devices SpectraMax M5e microplate reader (Sunnyvale, CA, USA). TEM images were taken by a JEOL JEM-2100 transmission electron microscope [UNIST Central Research Facilities (UCRF), Ulsan, Republic of Korea]. ESI–MS and IM–MS analyses were performed using a Waters Synapt G2-Si quadrupole time-of-flight (Q-Tof) ion mobility mass spectrometer (Waters, Manchester, UK) equipped with an ESI source [DGIST Center for Core Research Facilities (CCRF), Daegu, Republic of Korea]. ^{1}H and ^{13}C NMR spectra were recorded using a 400 MHz Agilent NMR spectrometer (UCRF). The high-resolution mass spectra of compounds were obtained through a Q exactive plus orbitrap mass spectrometer (Thermo Fisher Scientific, Carlsbad, CA, USA).

2.4.2. Preparation of 1

Ethylene sulfide (150 μL, 2.5 mmol) was added dropwise into a solution of dimethyl-4-phenylenediamine (690 mg, 5 mmol) in EtOH (3 mL) and the reaction mixture was heated to 100 °C under N_2 (g). After 2 h, ethylene sulfide (100 μL, 1.7 mmol) was added dropwise. After 1 h, the solvent was removed under vacuum. The residue was dissolved in water and extracted with ethyl acetate (EtOAc; 3x). The combined organic layer was dried over anhydrous magnesium sulfate

ULSAN NATIONAL INSTITUTE OF SCIENCE AND TECHNOLOGY

($MgSO_4$) and concentrated under the vacuum. The crude compound was purified by column chromatography (SiO_2; EtOAc:hexanes = 1:3) yielding a product (white oil; 140 mg, 0.71 mmol, 29%). ^{1}H NMR [400 MHz, CD_2Cl_2, δ (ppm)]: 6.71 (2H, d, J = 8.8 Hz), 6.61 (2H, d, J = 8.8 Hz), 3.57 (1H, br), 3.28 (2H, t, J = 6.4 Hz), 2.81, (6H, s), 2.73 (2H, m), 1.48 (1H, m). ^{13}C NMR [100 MHz, CD_2Cl_2, δ (ppm)]: 144.9, 140.1, 115.8, 115.0, 48.2, 42.2, 24.9. HRMS (*m/z*): $[M + H]^+$ Calcd. for $C_{10}H_{16}N_2S$, 197.1107; found, 197.1102.

2.4.3. Preparation of 2

4-Iodoaniline (660 mg, 3.0 mmol), 2-mercaptoethanol (0.42 mL, 6.0 mmol), copper sulfate pentahydrate ($CuSO_4 \cdot 5H_2O$; 38 mg, 0.15 mmol), and KOH (840 mg, 15 mmol) were added into a test tube containing DMSO/H_2O (2 mL/0.2 mL) with a magnetic stir bar. After flushing with Ar (g), the mixture was stirred in a preheated oil bath at 90 °C for 20 h and then cooled to room temperature. The reaction was quenched with water and extracted with EtOAc (4x). The organic layer was washed with water (1x) and brine (1x) and then concentrated under vacuum. The crude product was purified by column chromatography (SiO_2; EtOAc:hexanes = 1:1) yielding a primary amine product (yellow oil; 360 mg, 2.1 mmol, 70%).

A mixture of 3 M sulfuric acid (H_2SO_4; 1.2 mL, 3.4 mmol) and formaldehyde (aq, 37% w/w, 0.64 mL, 8.4 mmol) was cooled to 0 °C. A slurry of 2-((4-aminophenyl)thio)ethanol (360 mg, 2.1 mmol) and sodium borohydride ($NaBH_4$; 480 mg, 13 mmol) in tetrahydrofuran (THF; 5 mL) was added dropwise into the solution. After stirring the solution for 1 h, the reaction mixture was basified with 1 N sodium hydroxide (NaOH; aq) and then extracted with EtOAc (3x). The combined organic phase was washed with brine (1x), dried over anhydrous $MgSO_4$, and concentrated under vacuum. The crude compound was purified by column chromatography (SiO_2; EtOAc:hexanes = 1:1) yielding a tertiary amine product (white solid; 330 mg, 1.7 mmol, 79%).

A solution of 2-((4-(dimethylamino)phenyl)thio)ethanol (340 mg, 1.7 mmol) and thiourea (140 mg, 1.9 mmol) in HCl (aq) (0.6 mL) was stirred at 100 °C for 6 h. The reaction mixture was cooled to 50 °C. A solution of NaOH (aq; 20% w/w, 0.39 mL) was slowly added to the reaction solution, and then white solid precipitates were obtained. The reaction mixture was stirred at 70 °C for 1 h until the white precipitates disappeared. The reaction was quenched with water and extracted with EtOAc (3x). The organic layer was washed with brine (1x), dried over anhydrous $MgSO_4$, and concentrated under vacuum. The crude product was purified by column chromatography (SiO_2; EtOAc:hexanes = 1:2) yielding a thiol product (140 mg, 0.65 mmol, 12%). ^{1}H NMR [400 MHz, CD_2Cl_2 , δ (ppm)]: 7.31 (2H, d, J = 8.1 Hz), 6.65 (2H, d, J = 8.8 Hz), 2.94 (6H, s), 2.91 (2H, m) 2.62 (2H, m), 1.72 (1H, t, J = 8.1 Hz). ^{13}C NMR [100 MHz, CD_2Cl_2, δ (ppm)]: 150.8, 135.0, 119.3, 113.1, 41.1, 40.5, 24.7. HRMS (*m/z*): $[M + H]^+$ Calcd. for $C_{10}H_{15}NS_2$, 214.0719; found, 214.0714.

2.4.4. Preparation of 3

4-Iodo-*N*,*N*-dimethylaniline (490 mg, 2.0 mmol), 2-(Boc-amino)ethanethiol (680 μL, 4.0 mmol), copper acetate dihydrate [$Cu(OAc)_2 \cdot 2H_2O$; 40 mg, 0.2 mmol], and potassium carbonate (K_2CO_3; 1.1 g, 8.0 mmol) were added into a test tube containing DMSO/H_2O (3 mL/1 mL) with a magnetic stir bar. After flushing with Ar (g), the mixture was stirred in a preheated oil bath at 90 °C for 24 h. After cooling the solution to room temperature, the reaction was quenched with EtOAc. The reaction solution was washed with water (3x) and brine (1x). The organic layer was dried over anhydrous $MgSO_4$ and concentrated under vacuum. The crude product was purified by column chromatography (SiO_2; EtOAc:hexanes = 1:10) yielding a product (white solid; 210 mg, 0.71 mmol, 34%).

tert-Butyl 2-(4-(dimethylamino)phenylthio)ethylcarbamate (400 mg, 1.4 mmol) was added into the solution of HCl/dioxane (4.0 M, 10 mL) at 0 °C under Ar (g). The reaction mixture was stirred at room temperature for 24 h. The solvent was removed under vacuum and the residue was washed with diethyl ether (Et_2O). The sticky compound was basified with 1 N NaOH (aq) and extracted with EtOAc (3x). The combined organic layer was washed with brine (1x), dried over anhydrous $MgSO_4$, and concentrated under vacuum. The crude compound was purified by column chromatography (SiO_2; CH_2Cl_2:CH_3OH = 7:1). A product (white powder; 50 mg, 0.25 mmol, 18%) was obtained by addition of Et_2O to the yellow liquid product. ^{1}H NMR [400 MHz, CD_3OD, δ (ppm)]: 7.35 (2H, m), 6.72 (2H, d, J = 8.8 Hz), 2.94 (10H, m), 1.90 (2H, s). ^{13}C NMR [100 MHz, CD_3OD, δ (ppm)]: 152.2, 136.0, 119.2, 114.2, 40.6. 39.8, 35.5. HRMS (*m/z*): $[M + H]^+$ Calcd. for $C_{10}H_{16}N_2S$, 197.1107; found, 197.1103.

2.4.5. Metal Binding Studies

The interactions of compounds with metal ions [Cu(II) and Zn(II)] were determined using UV–visible spectroscopy (UV–Vis). The solutions of compounds (50 μM; 1% v/v DMSO) were prepared in EtOH for [Cu(II) samples] or buffer [20 μM HEPES, pH 7.4, 150 μM NaCl; for Zn(II) samples). Various concentrations of $CuCl_2$ or $Zn(NO_3)_2$ (25, 50, 100, and 250 μM) were titrated to the solutions of the compound. The UV–Vis spectra were recorded after 10 min incubation for every titration at room temperature.

2.4.6. Cyclic Voltammetry (CV)

Cyclic voltammograms were recorded under N_2 (g) with a CHI620E model potentiostat (Qrins) with three electrodes composed of an Ag/AgCl reference electrode [RE-1B Reference electrode (Ag/AgCl); Qrins], a Pt wire auxiliary electrode (SPTE Platinum electrode; Qrins), and a glassy carbon working electrode (Qrins). Electrochemical analyses of compounds (dissolved in DMSO; final concentration, 1 mM) were recorded in 0.1 M *tetra*-*N*-butylammonium perchlorate (in DMSO) and 1 M NaCl (in

ULSAN NATIONAL INSTITUTE OF SCIENCE AND TECHNOLOGY

ddH_2O; 1% v/v DMSO) at various scan rates (25, 50, 100, 150, 200, and 250 mV/s) at room temperature.

2.4.7. DTNB Assay

The oxidation of a thiol group in our compounds was evaluated through the DTNB assay [DTNB = 5,5'-dithio-bis-(2-nitrobenzoic acid)]. The solutions of DTNB (50 μM) were prepared in 0.1 M sodium phosphate buffer, pH 8.0, 1 mM EDTA, followed by treatment of *L*-cysteine, as a positive control, and small molecules (50 μM; 1% v/v DMSO). The DTNB molecule can react with the thiol groups in small molecules, yielding a product containing a newly formed disulfide bond and a yellow-colored compound, 2-nitro-5-thiobenzoic acid dianion (TNB^{2-}).[64] After 15 min incubation at room temperature, the absorbance of TNB^{2-} at 412 nm was measured.

2.4.8. Stability of Compounds

The oxidation of compounds was traced by UV–Vis. The solutions of compounds (50 μM; 1% v/v DMSO) were prepared in buffer (20 μM HEPES, pH 7.4, 150 μM NaCl). The compound was incubated for 24 h at room temperature without agitation.

2.4.9. TEAC Assay

The assay employing Neuro2a (N2a) cell lysates was conducted following the previously reported methods.[34,63] Cell lysates were prepared following a previously reported procedure with modifications.[65] N2a cells were seeded in a six-well plate and grown to approximately 80-90% confluence. Cells were washed once with cold phosphate buffered saline (PBS, pH 7.4, GIBCO, Grand Island, NY, USA) and harvested by gently pipetting off adherent cells with cold PBS. The cell pellet was generated by centrifugation (2,000 g for 10 min at 4 °C) and sonicated on ice (5 s pulses, 3x with 20 s intervals between each pulse) in 2 mL of cold buffer (5 mM potassium phosphate, pH 7.4, containing 0.9% NaCl and 0.1% glucose). The cell lysates were centrifuged at 5,000 g for 10 min at 4 °C. The supernatant was removed and stored on ice until use. To prepare the standard and samples in 96 well plates, 10 μL of the supernatant of cell lysates was delivered followed by the addition of compound (10 μL), metmyoglobin (55 μM, 10 μL), 2,2'-azino-bis(3-ethylbenzothiazoline-6-sulphonic acid) (ABTS; 220 μM, 150 μL), and H_2O_2 (412 μM, 40 μL) in order. The final concentrations (2.14, 4.28. 6.43, 8.57, 10.7, and 15.7 μM) of compounds and Trolox were used. After 5 min incubation at room temperature, the absorbance at 750 nm was recorded. The percent inhibition was calculated according to the measured absorbance [% inhibition = $100 \times (A_0 - A)/A_0$, where A and A_0 are the absorbance of the supernatant of cell lysates with and without compound treatment, respectively] and was plotted as a function of compound concentration. The TEAC values of

ULSAN NATIONAL INSTITUTE OF SCIENCE AND TECHNOLOGY

compounds for each time point were calculated as a ratio of the slope of the compound to that of Trolox. The measurements were conducted in triplicate.

2.4.10. Aβ Aggregation Experiments

$A\beta_{40}$ or $A\beta_{42}$ was dissolved in ammonium hydroxide [NH_4OH (aq); 1% v/v]. The resulting solution was aliquoted, lyophilized overnight, and stored at –80 °C. A stock solution of Aβ was then prepared by dissolving the lyophilized peptide using NH_4OH (1% v/v, 10 μL) and diluting with ddH_2O. All Aβ samples were prepared by following the previously reported procedures.[34,37,66,67] The concentration of the peptide solution was determined by measuring the absorbance of the solution at 280 nm (ε = 1,450 $M^{-1}cm^{-1}$ for $A\beta_{40}$; ε = 1,490 $M^{-1}cm^{-1}$ for $A\beta_{42}$). The peptide stock solution was diluted to a final concentration of 25 μM in the Chelex-treated buffer [20 μM HEPES, pH 6.6 [for Cu(II) samples] and pH 7.4 [for metal-free and Zn(II) samples], 150 μM NaCl]. For inhibition studies, compounds (final concentration, 50 μM; 1% v/v DMSO) were added to the samples of Aβ (25 μM) in the absence and presence of a metal chloride salt ($CuCl_2$ or $ZnCl_2$; 25 μM) followed by incubation at 37 °C with constant agitation for 24 h. For disaggregation studies, Aβ (25 μM) was incubated with and without a metal chloride salt ($CuCl_2$ or $ZnCl_2$; 25 μM) for 24 h at 37 °C with constant agitation to generate preformed Aβ aggregates. The resulting peptide aggregates were then treated with compounds (50 μM) and incubated with constant agitation for an additional 24 h.

2.4.11. Gel Electrophoresis with Western Blotting (Gel/Western Blot)

The Aβ resultant species from *in vitro* experiments were analyzed through gel electrophoresis with Western blotting (gel/Western blot) using an anti-Aβ antibody (6E10).[34,37,66,67] The samples (10 μL) were separated on a 10-20% Tris-tricine gel (Thermo Fisher Scientific). Following separation, the proteins were transferred onto nitrocellulose membranes and blocked with bovine serum albumin (BSA, 3% w/v, Sigma-Aldrich) in Tris-buffered saline (TBS) containing 0.1% Tween-20 (TBS-T) for 2 h (at room temperature) or overnight (at 4 °C). The membranes were incubated with the anti-Aβ antibody (6E10) (1:2,000, Covance, Princeton, NJ, USA) in a solution of 2% BSA (w/v in TBS-T) for 4 h (at room temperature) or overnight (at 4 °C). After washing with TBS-T (3x, 10 min), a horseradish peroxidase-conjugated goat anti-mouse secondary antibody (1:5,000 in 2% w/v BSA in TBS-T; Cayman Chemical Company) was added for 1.5 h at room temperature. A homemade ECL kit[63,68,69] was used to visualize gel/Western blot data on a ChemiDoc MP Imaging System (Bio-Rad, Hercules, CA, USA).

2.4.12. Transmission Electron Microscopy (TEM)

Samples for TEM were prepared according to previously reported methods.[34,37,63,66-68] Glow-

ULSAN NATIONAL INSTITUTE OF SCIENCE AND TECHNOLOGY

discharged grids (Formvar/Carbon 300-mesh, Electron Microscopy Sciences, Hatfield, PA, USA) were treated with Aβ samples (25 μM, 5 μL) for 2 min at room temperature. Excess sample was removed using filter paper followed by washing twice with ddH_2O. Each grid, incubated with uranyl acetate (1%, ddH_2O, 5 μL) for 1 min, was blotted off and dried for 15 min at room temperature. Images for each sample were taken on a JEOL JEM-2100 transmission electron microscope (200 kV; 25,000x magnification; UCRF).

2.4.13. MTT Assay

The SH-SY5Y (5Y) cell line was purchased from the American Type Culture Collection (ATCC, Manassas, VA, USA). The cell line was maintained in media containing 50% minimum essential medium (MEM) and 50% F12 (GIBCO) and supplemented with 10% fetal bovine serum (Sigma-Aldrich), 100 U/mL penicillin, and 100 mg/mL streptomycin (GIBCO). Cells were grown and maintained at 37 °C in a humidified atmosphere with 5% CO_2. The cells used for our studies did not indicate mycoplasma contamination. Cell viability upon treatment with compounds was determined by the MTT assay [MTT = 3-(4,5-dimethylthiazol-2-yl)-2,5-diphenyltetrazolium bromide]. Cells were seeded in a 96 well plate (15,000 cells in 100 μL per well) and treated with Aβ (10 μM) with or without $CuCl_2$ or $ZnCl_2$ (5 μM), followed by addition of compounds (10 μM, 1% v/v DMSO). After 24 h incubation, MTT [25 μL of 5 mg/mL in PBS (pH 7.4, GIBCO)] was added to each well, and the plate was incubated for 4 h at 37 °C. Formazan produced by cells was solubilized using an acidic solution of DMF (pH 4.5, 50% v/v, aq) and sodium dodecyl sulfate (SDS; 20% w/v) overnight at room temperature in the dark. The absorbance was measured at 600 nm by the microplate reader. Cell viability was calculated relative to cells containing an equivalent amount of DMSO.

2.4.14. Electrospray Ionization Ion Mobility Mass Spectrometry (ESI–IM–MS)

The experiments were performed according to previously reported methods.[63,68,70] $A\beta_{40}$ and $A\beta_{42}$ (100 μM) were incubated with compounds (500 μM; 1% v/v DMSO) and/or $CuCl_2$ (100 μM) in 20 mM ammonium acetate (pH 7.2) at 37 °C without agitation. Incubated samples were diluted by 10 fold with water and then injected into the mass spectrometer. A Waters Synapt G2-Si quadrupole time-of-flight (Q-Tof) ion mobility mass spectrometer (Waters) equipped with ESI source (CCRF) was used for the experiments. The capillary voltage, sampling cone voltage, and source temperature were set to 2.8 kV, 70 V, and 40 °C, respectively. The backing pressure was adjusted to 2.7 mbar. Ion mobility wave height and velocity were adjusted to 10 V and 300 m/s, respectively, and gas flow for the helium and ion mobility cell was set to 120 and 30 mL/min, respectively. Tandem MS (ESI–MS^2) analyses were additionally performed on the singly oxidized Aβ and complexes of Aβ with compounds. The ESI parameters and experimental conditions were the same as above. Collision-induced dissociation

ULSAN NATIONAL INSTITUTE OF SCIENCE AND TECHNOLOGY

(CID) was conducted by applying the collision energy in the trap and adjusting the low mass (LM) resolution to 10 or 15 depending on the samples. More than 200 spectra were obtained for each sample and were averaged for the analyses. To estimate the collision cross section (CCS) values of IM–MS data, the calibration was also carried out base on the previously reported methods.[71]

2.4.15. Parallel Artificial Membrane Permeability Assay Adapted for the Blood-brain Barrier (PAMPA–BBB)

PAMPA–BBB experiments were conducted using the PAMPA Explorer kit (*p*ION Inc., Billerica, MA, USA) using previously reported protocols.[2,5,6] The compounds (25 μM, 200 μL) in Prisma HT buffer (pH 7.4, *p*ION) were added to the wells of a donor plate (number of replicates = 12). The polyvinylidene fluoride (PVDF, 0.45 μM) filter membrane on the acceptor plate was coated with BBB-1 lipid formulation (5 μL, *p*ION). The acceptor plate was then placed on the top of the donor plate. Brain sink buffer (BSB, 200 μL, *p*ION) was added to each well of the acceptor plate and was incubated for 4 h at room temperature without agitation. UV–Vis spectra of the solutions in the reference, acceptor, and donor plates were measured using the microplate reader. The PAMPA Explorer software v. 3.5 (*p*ION) was used to calculate the $-\log P_e$ values for compounds. CNS±designations were assigned by comparison with compounds that were identified in previous reports.[72,73]

2.5. Acknowledgments

This work was supported by the National Research Foundation of Korea (NRF) grant funded by the Korean government [NRF-2016R1A5A1009405 and NRF-2017R1A2B3002585 (to M.H.L.); NRF-2015R1D1A1A01060188 (to J.C.)]; the DGIST R&D Program (17-BD-0403) (to J.C.).

2.6. References

1. Jakob-Roetne, R.; Jacobsen, H. *Angew. Chem. Int. Ed.* **2009**, *48*, 3030–3059.
2. Kepp, K. P. *Chem. Rev.* **2012**, *112*, 5193–5239.
3. Faller, P.; Hureau, C. *Dalton Trans.* **2009**, *7*, 1080–1094.
4. Hureau, C.; Faller, P. *Biochimie* **2009**, *91*, 1212–1217.
5. Faller, P.; Hureau, C.; Berthoumieu, O. *Inorg. Chem.* **2013**, *52*, 12193–12206.
6. Markesbery, W. R. *Free Radic. Biol. Med.* **1997**, *23*, 134–147.
7. Beck, M. W.; Pithadia, A. S.; DeToma, A. S.; Korshavn, K. J.; Lim, M. H. *Ligand design in medicinal inorganic chemistry*, Storr, T. Ed.; Wiley: Chichester, 2014; ch. 10, pp 257–286.
8. Derrick, J. S.; Lim, M. H. *ChemBioChem* **2015**, *16*, 887–898.
9. DeToma, A. S.; Salamekh, S.; Ramamoorthy, A.; Lim, M. H. *Chem. Soc. Rev.* **2012**, *41*, 608–621.

ULSAN NATIONAL INSTITUTE OF SCIENCE AND TECHNOLOGY

10. Savelieff, M. G.; Lee, S.; Liu, Y.; Lim, M. H. *ACS Chem. Biol.* **2013**, *8*, 856–865.
11. Kotler, S. A.; Walsh, P.; Brender, J. R.; Ramamoorthy, A. *Chem. Soc. Rev.* **2014**, *43*, 6692–6700.
12. Lee, S. J. C.; Nam, E.; Lee, H. J.; Savelieff, M. G.; Lim, M. H. *Chem. Soc. Rev.* **2017**, *46*, 310–323.
13. Savelieff, M. G.; DeToma, A. S.; Derrick, J. S.; Lim, M. H. *Acc. Chem. Res.* **2014**, *47*, 2475–2482.
14. Shearer, J.; Callan, P. E.; Tran, T.; Szalai, V. A. *Chem. Commun.* **2010**, *46*, 9137–9139.
15. Peck, K. L.; Clewett, H. S.; Schmitt, J. C.; Shearer, J. *Chem. Commun.* **2013**, *49*, 4797–4799.
16. Smith, D. G.; Cappai, R.; Barnham, K. J. *Biochim. Biophys. Acta.* **2007**, *1768*, 1976–1990.
17. Perry, G.; Cash, A. D.; Smith, M. A. *J. Biomed. Biotechnol.* **2002**, *2*, 120–123.
18. Sayre, L. M.; Perry, G.; Smith, M. A. *Chem. Res. Toxicol.* **2008**, *21*, 172–188.
19. Alzheimer's Association, *Alzheimers Dement* **2017**, *13*, 325–373.
20. Lorenzo, A.; Yankner, B. A. *Proc. Natl. Acad. Sci. U. S. A.* **1994**, *91*, 12243–12247.
21. Nie, Q.; Du, X.; Geng, M.-Y. *Acta Pharmacol. Sin.* **2011**, *32*, 545–551.
22. Fulop, L.; Mandity, I. M.; Juhasz, G.; Szegedi, V.; Hetenyi, A.; Weber, E.; Bozso, Z.; Simon, D.; Benko, M.; Kiraly, Z.; Martinek, T. A. *PLoS One* **2012**, *7*, e39485.
23. Jones, M. R.; Service, E. L.; Thompson, J. R.; Wang, M. C. P.; Kimsey, I. J.; DeToma, A. S.; Ramamoorthy, A.; Lim, M. H.; Storr, T. *Metallomics* **2012**, *4*, 910–920.
24. Choi, J.-S.; Braymer, J. J.; Nanga, R. P.; Ramamoorthy, A.; Lim, M. H. *Proc. Natl. Acad. Sci. USA* **2010**, *107*, 21990–21995.
25. Ji, Y.; Lee, H. J.; Kim, M.; Nam, G.; Lee, S. J. C.; Cho, J.; Park, C.-M.; Lim, M. H. *Inorg. Chem.* **2017**, *56*, 6695–6705.
26. Feng, Y.; Wang, X. *Oxid. Med. Cell. Longev.* **2012**, *2012*, 472932.
27. de Oliveira, B. F.; Veloso, C. A.; Nogueira-Machado, J. A.; de Moraes, E. N.; dos Santos, R. R.; Cintra, M. T.; Chaves, M. M. *Nutr. Neurosci.* **2012**, *15*, 244–251.
28. Wu, W.; Lei, P.; Liu, Q.; Hu, J.; Gunn, A. P.; Chen, M.; Rui, Y.-F.; Su, X.; Xie, Z.; Zhao, Y.-F.; Bush, A. I.; Li, Y. *J. Biol. Chem*. **2008**, *283*, 31657–31664.
29. Hamaguchi, T.; Ono, K.; Yamada, M. *Cell. Mol. Life Sci.* **2006**, *63*, 1538–1552.
30. Schugar, H.; Green, D. E.; Bowen, M. L.; Scott, L. E.; Storr, T.; Bohmerle, K.; Thomas, F.; Allen, D. D.; Lockman, P. R.; Merkel, M.; Thompson, K. H.; Orvig, C. *Angew. Chem. Int. Ed.* **2007**, *46*, 1716–1718.
31. Dickens, M. G.; Franz, K. J. *ChemBioChem* **2010**, *11*, 59–62.
32. Lincoln, K. M.; Richardson, T. E.; Rutter, L.; Gonzalez, P.; Simpkins, J. W.; Green, K. N. *ACS Chem. Neurosci.* **2012**, *3*, 919–927.
33. Sharma, A. K.; Pavlova, S. T.; Kim, J.; Finkelstein, D.; Hawco, N. J.; Rath, N. P.; Kim, J.; Mirica, L. M. *J. Am. Chem. Soc.* **2012**, *134*, 6625–6636.

ULSAN NATIONAL INSTITUTE OF SCIENCE AND TECHNOLOGY

34. Lee, S.; Zheng, X.; Krishnamoorthy, J.; Savelieff, M. G.; Park, H. M.; Brender, J. R.; Kim, J. H.; Derrick, J. S.; Kochi, A.; Lee, H. J.; Kim, C.; Ramamoorthy, A.; Bowers, M. T.; Lim, M. H. *J. Am. Chem. Soc.* **2014**, *136*, 299–310.
35. Mao, F.; Yan, J.; Li, J.; Jia, X.; Miao, H.; Sun, Y.; Huang, L.; Li, X. *Org. Biomol. Chem.* **2014**, *12*, 5936–5944.
36. Gonzalez, P.; da Costa, V. C. P.; Hyde, K.; Wu, Q.; Annunziata, O.; Rizo, J.; Akkaraju, G.; Green, K. N. *Metallomics* **2014**, *6*, 2072–2082.
37. Derrick, J. S.; Kerr, R. A.; Nam, Y.; Oh, S. B.; Lee, H. J.; Earnest, K. G.; Suh, N.; Peck, K. L.; Ozbil, M.; Korshavn, K. J.; Ramamoorthy, A.; Prabhakar, R.; Merino, E. J.; Shearer, J.; Lee, J.-Y.; Ruotolo, B. T.; Lim, M. H. *J. Am. Chem. Soc.* **2015**, *137*, 14785–14797.
38. Folk, D. S.; Franz, K. J. *J. Am. Chem. Soc.* **2010**, *132*, 4994–4995.
39. Beck, M. W.; Derrick, J. S.; Kerr, R. A.; Oh, S. B.; Cho, W. J.; Lee, S. J. C.; Ji, Y.; Han, J.; Tehrani, Z. A.; Suh, N.; Kim, S.; Larsen, S. D.; Kim, K. S.; Lee, J.-Y.; Ruotolo, B. T.; Lim, M. H. *Nat. Commun.* **2016**, *7*, 13115.
40. Biancalana, M.; Koide, S. *Biochim. Biophys. Acta* **2010**, *1804*, 1405–1412.
41. Bussiere, T.; Bard, F.; Barbour, R.; Grajeda, H.; Guido, T.; Khan, K.; Schenk, D.; Games, D.; Seubert, P.; Buttini, M. *Am. J. Pathol.* **2004**, *165*, 987–995.
42. Banks, C. E.; Lawrence, N. S.; Compton, R. G. *Electroanal.* **2003**, *15*, 243–248.
43. Nickel, U.; Garcia-Angel, M. G.; Ramminger, U.; Weidinger, B. *Z. Phys. Chem.* **2006**, *220*, 497–509.
44. Beck, M. W.; Derrick, J. S.; Suh, J.-M.; Kim, M.; Korshavn, K. J.; Kerr, R. A.; Cho, W. J.; Larsen, S. D.; Ruotolo, B. T.; Ramamoorthy, A.; Lim, M. H. *ChemMedChem* **2017**, *12*, 1–12.
45. Kepp, K. P. *Coord. Chem. Rev.* **2017**, *351*, 127–159.
46. Pearson, R. G. *J. Am. Chem. Soc.* **1963**, *85*, 3533–3539.
47. Chevion, S.; Roberts, M. A.; Chevion, M. *Free. Radic. Biol. Med.* **2000**, *28*, 860–870.
48. Watson, A. A.; Fairlie, D. P.; Craik, D. J. *Biochemistry* **1998**, *37*, 12700–12706.
49. Brown, A. M.; Lemkul, J. A.; Schaum, N.; Bevan, D. R. *Arch. Biochem. Biophys.* **2014**, *545*, 44–52.
50. Bitan, G.; Tarus, B.; Vollers, S. S.; Lashuel, H. A.; Condron, M. M.; Straub, J. E.; Teplow, D. B. *J. Am. Chem. Soc.* **2003**, *125*, 15359–15365.
51. Kang, J.; Lee, S. J. C.; Nam, J. S.; Lee, H. J.; Kang, M.-G.; Korshavn, K. J.; Kim, H.-T.; Cho, J.; Ramamoorthy, A.; Rhee, H.-W.; Kwon, T.-H.; Lim, M. H. *Chem. Eur. J.* **2017**, *23*, 1645–1653.
52. Cheignon, C.; Faller, P.; Testemale, D.; Hureau, C.; Collin, F. *Metallomics* **2016**, *8*, 1081–1089.
53. Dean, R. T.; Fu, S.; Stocker, R.; Davies, M. J. *Biochem. J.* **1997**, *324*, 1–18.
54. Inoue, K.; Nakagawa, A.; Hino, T.; Oka, H. *Anal. Chem.* **2009**, *81*, 1819–1825.
55. Hou, L.; Shao, H.; Zhang, Y.; Li, H.; Menon, N. K.; Neuhaus, E. B.; Brewer, J. M.; Byeon, I.-J.

ULSAN NATIONAL INSTITUTE OF SCIENCE AND TECHNOLOGY

L.; Ray, D. G.; Vitek, M. P.; Iwashita, T.; Makula, R. A.; Przybyla, A. B.; Zagorski, M. G. *J. Am. Chem. Soc.* **2004**, *126*, 1992–2005.

56. Suprun, E. V.; Khmeleva, S. A.; Radko, S. P.; Kozin, S. A.; Archakov, A. I.; Shumyantseva, V. V. *Electrochem. Commun.* **2016**, *65*, 53–56.
57. Schoneich, C.; Williams, T. D. *Chem. Res. Toxicol.* **2002**, *15*, 717–722.
58. Glass, R. S. *Organosulfur Chemistry II*, ed. P. C. B. Page, P. C. B. Ed.; Springer: Berlin, 1999, pp 1–87.
59. Hartley, D. M.; Walsh, D. M.; Ye, C. P.; Diehl, T.; Vasquez, S.; Vassilev, P. M.; Teplow, D. B.; Selkoe, D. J. *J. Neurosci.* **1999**, *19*, 8876–8884.
60. Klug, G. M. J. A.; Losic, D.; Subasinghe, S. S.; Aguilar, M.-I.; Martin, L. L.; Small, D. H. *Eur. J. Biochem.* **2003**, *270*, 4282–4293.
61. Huang, D.; Ou, B.; Prior, R. L. *J. Agric. Food Chem.* **2005**, *53*, 1841–1856.
62. Re, R.; Pellegrini, N.; Proteggente, A.; Pannala, A.; Yang, M.; Rice-Evans, C. *Free. Radic. Biol. Med.* **1999**, *26*, 1231–1237.
63. Lee, H. J.; Korshavn, K. J.; Nam, Y.; Kang, J.; Paul, T. J.; Kerr, R. A.; Youn, I. S.; Ozbil, M.; Kim, K. S.; Ruotolo, B. T.; Prabhakar, R.; Ramamoorthy, A.; Lim, M. H. *Chem. Eur. J.* **2017**, *23*, 2706–2715.
64. Riddles, P. W.; Blakeley, R. L.; Zerner, B. *Anal. Biochem.* **1979**, *94*, 75–81.
65. Spencer, V. A.; Sun, J. M.; Li, L.; Davie, J. R. *Methods* **2003**, *31*, 67–75.
66. Choi, J.-S.; Braymer, J. J.; Nanga, R. P. R.; Ramamoorthy, A.; Lim, M. H. *Proc. Natl. Acad. Sci. U. S. A.* **2010**, *107*, 21990–21995.
67. Hindo, S. S.; Mancino, A. M.; Braymer, J. J.; Liu, Y.; Vivekanandan, S.; Ramamoorthy, A.; Lim, M. H. *J. Am. Chem. Soc.* **2009**, *131*, 16663–16665.
68. Beck, M. W.; Oh, S. B.; Kerr, R. A.; Lee, H. J.; Kim, S. H.; Kim, S.; Jang, M.; Ruotolo, B. T.; Lee, J.-Y.; Lim, M. H. *Chem. Sci.* **2015**, *6*, 1879–1886.
69. Mruk, D. D.; Cheng, C. Y. *Spermatogenesis* **2011**, *1*, 121–122.
70. Hyung, S. J.; DeToma, A. S.; Brender, J. R.; Lee, S.; Vivekanandan, S.; Kochi, A.; Choi, J.-S.; Ramamoorthy, A.; Ruotolo, B. T.; Lim, M. H. *Proc. Natl. Acad. Sci. U. S. A.* **2013**, *110*, 3743–3748.
71. Ruotolo, B. T.; Benesch, J. L.; Sandercock, A. M.; Hyung, S. J.; Robinson, C. V. *Nat. Protoc.* **2008**, *3*, 1139–1152.
72. Di, L.; Kerns, E. H.; Fan, K.; McConnell, O. J.; Carter, G. T. *Eur. J. Med. Chem.* **2003**, *38*, 223–232.
73. Avdeef, A.; Bendels, S.; Di, L.; Faller, B.; Kansy, M.; Sugano, K.; Yamauchi, Y. *J. Pharm. Sci.* **2007**, *96*, 2893–2909.

ULSAN NATIONAL INSTITUTE OF SCIENCE AND TECHNOLOGY

Chapter 3.

Detection of Metal Ions in Living Cells by Fluorescence-based Chemosensors

The results presented in this chapter were published; (1) Jo, T. G.; Bok, K. H.; Han, J.; Lim, M. H.; Kim, C. *Dyes Pigm.* **2017**, *139*, 136–147; (2) Jeong, H. Y.; Lee, S. Y.; Han, J.; Lim, M. H.; Kim, C. *Tetrahedron* **2017**, *73*, 2690–2697; (3) Jo, T. G.; Jung, J. M.; Han, J.; Lim, M. H.; Kim, C. *RSC Adv.* **2017**, *7*, 28723–28732. I conducted the imaging experiments in order to monitor fluorescent responses of chemosensors for metal ions in living cells.

ULSAN NATIONAL INSTITUTE OF SCIENCE AND TECHNOLOGY

3.1. Introduction

Dyshomeostasis of transition metal ions has been suggested to be involved in the pathogenesis of neurodegenerative diseases including Alzheimer's disease (AD) and Parkinson's disease (PD).[1,2] Particularly, aluminum, the third most prevalent metallic elements in the earth, can be accumulated in the regions of the brain, *i.e.*, the cortex and hippocampus, both of which are notably vulnerable at the early stage of AD.[1,2] Recent studies have revealed that a trace amount of Al(III), transported to the brain *via* blood-brain barrier (BBB), can either intrude metal-mediated signaling pathways [*e.g.*, Ca(II) exchange] or replace essential biometals in transporters (*e.g.*, iron carrier transferrin), which induces neurotoxicity.[3,4] In addition, Al(III) can interfere the activities of iron-sulfur clusters in mitochondrial respiratory systems, disrupting the energy production.[5,6] Moreover, Al(III) has been reported to directly bind Aβ and stabilize structured oligomers.[5,6] In order to quantify the concentration of Al(III) and monitor its compartmentalization in the brain, various chemosensors able to specifically detect this metal ion would be valuable.[2,7,8] In this Chapter, we described three chemical tools capable of targeting Al(III) in living cells.

3.2. Results and Discussions

3.2.1. Fluorescent Responses of AIC-Jul to Al(III) in Living Cells

Scheme 3.1. Proposed structure of the **AIC-Jul**–Al(III) complex.

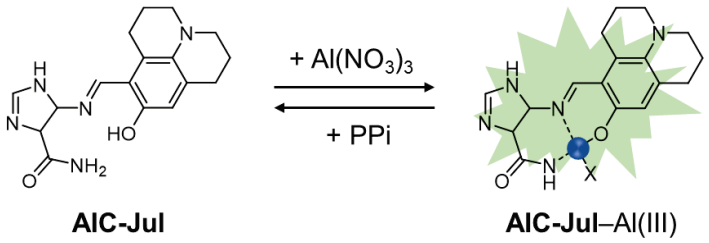

AIC-Jul was rationally designed through the incorporation of imidazole and julolidine (Scheme 3.1).[9] This molecule functions as a turn-on and turn-off fluorescent sensors against Al(III) and pyrophosphate ($P_2O_7^{4-}$, PPi), the product of during hydrolysis of adenosine triphosphate (ATP), respectively. Upon incubation of **AIC-Jul** (20 μM, DMSO 1%, v/v) with 5 and 10 equiv of Al(III) for 10 min, significant fluorescent responses were monitored employing the green fluorescence protein (GFP) channel [excitation 470 (± 11) nm; emission 510 (± 21) nm; Figure 3.1a]. Furthermore, the **AIC-Jul**–Al(III) complex was shown to specifically detect PPi among various anions (*e.g.*, Cl^-, F^-, N_3^-, and NO_3^-) in the cellular environment. When PPi was treated to cells, pre-incubated with **AIC-Jul** and Al(III), the Al(III)–PPi complex was subsequently formed, indicative of detaching Al(III) from the complex. The quenching process achieved *via* complexation of Al(III)–PPi was monitored using the GFP channel (Figure 3.1b). Our experiments demonstrate the potential of **AIC-Jul** as a sensor for

ULSAN NATIONAL INSTITUTE OF SCIENCE AND TECHNOLOGY

both AI(III) and PPi in living cells.

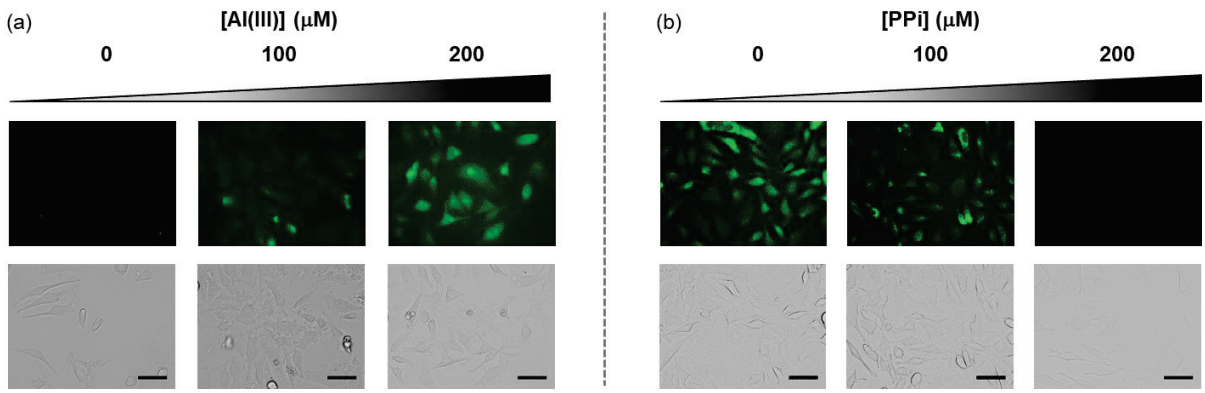

Figure 3.1. Fluorescent responses of **AIC-Jul** to Al(III) in HeLa cells in the absence and presence of PPi. (a) Cells were pre-incubated with **AIC-Jul** for 10 min prior to addition of various concentrations of Al(III). (b) Cells incubated with **AIC-Jul** (for 5 min) followed by addition of Al(III) for 10 min were treated with various concentrations of PPi. Conditions: [**AIC-Jul**] = 20 μM; [Al(III)] = 0, 100, and 200 μM; [PPi] = 0, 100, and 200 μM; 37 °C; 5% CO_2. The scale bar is 50 μm.

3.2.2. Fluorescent Responses of TP-DAS to Al(III) in Living Cells

Scheme 3.2. Proposed structure of the **TP-DAS**–Al(III) complex.

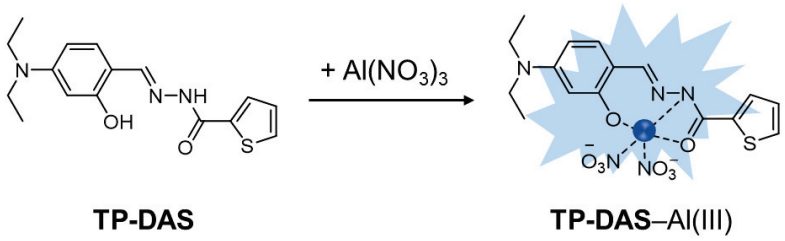

TP-DAS was newly designed by introduction of diethylaminophenol and thiophene into a framework (Scheme 3.2).[10] Based on competition experiments, Co(II), Ni(II), and Zn(II) could not interfere the interactions between **TP-DAS** and Al(III), while Cu(II) and Fe(II/III) were shown to intrinsically quench the fluorescent responses from the **TP-DAS**–Al(III) complex. Our compound (5 μM, DMSO 1%, v/v) was incubated with Al(III) in HeLa cells for 10 min at various concentrations (Figure 3.2). The fluorescent responses of **TP-DAS** as a function of the concentration of Al(III) were gradually enhanced, monitored at the channel of 4',6-diamidino-2-phenylindole (DAPI) channel [excitation 357 (± 22) nm; emission 447 (± 30) nm]. Our experimental results reveal that **TP-DAS** could be a detector for Al(III) in biological systems.

ULSAN NATIONAL INSTITUTE OF SCIENCE AND TECHNOLOGY

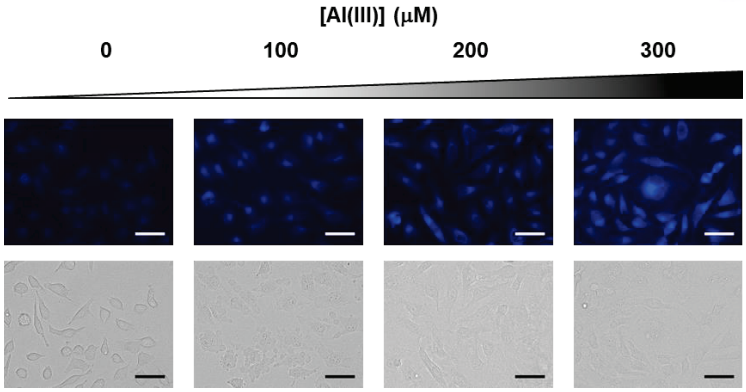

Figure 3.2. Fluorescent responses of **TP-DAS** to Al(III) in HeLa cells. Cells were pre-incubated with **TP-DAS** for 10 min prior to addition of various concentrations of Al(III). Conditions: [**TP-DAS**] = 5 μM; [Al(III)] = 0, 100, 200, and 300 μM; 37 °C; 5% CO_2. The scale bar is 50 μm.

3.2.3. Fluorescent Responses of Sul-Nap to Al(III) in Living Cells

Scheme 3.3. Proposed structure of the **Sul-Nap**–Al(III) complex.

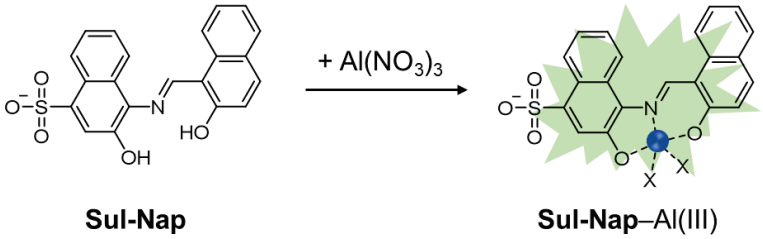

Sul-Nap was rationally designed by integrating a water-soluble sulfonic acid group to the naphthol moiety, a widely utilized fluorophore (Scheme 3.3).[11] **Sul-Nap** was presented to selectively recognize Al(III) in a 1:1 ratio, followed by a significant change in fluorescence emission in aqueous media. In order to examine the potentials of **Sul-Nap** to be used for sensing Al(III) in biological systems, fluorescence imaging experiments were performed (Figure 3.3). HeLa cells were incubated with **Sul-Nap** (20 μM, DMSO 1%, v/v) for 10 min, prior to treatment of 5 equiv of Al(III) for additional 10 min. The fluorescence responses of **Sul-Nap** in the presence of Al(III) were detected at the GFP channel [excitation 470 (± 11) nm; emission 510 (± 21) nm]. Note that due to the poor cell permeability of the molecule, the concentration-dependent fluorescent responses of **Sul-Nap** to Al(III) could not be monitored (Figure 3.3).

ULSAN NATIONAL INSTITUTE OF SCIENCE AND TECHNOLOGY

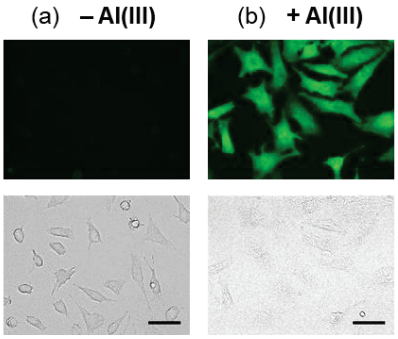

Figure 3.3. Fluorescent responses of **Sul-Nap** in HeLa cells in the (a) absence and (b) presence of Al(III). Cells were pre-incubated with **Sul-Nap** for 10 min prior to addition of Al(III). Conditions: [**Sul-Nap**] = 20 μM; [Al(III)] = 100 μM; 37 C; 5% CO_2. Scale bar = 50 μm.

3.3. Conclusions

Impaired homeostasis of metal ions is found in the AD-affected brain.[1,2] In the recent studies, Al(III) has been suggested as an additional risk factor in AD, which can facilitate Aβ aggregation and interfere the activities of metalloenzymes.[3,4] In order to gain a better understanding of Al(III) in AD, the design of small molecules able to trace this metal ion would be desirable. In this Chapter, we developed three chemical probes, **AIC-Jul**, **TP-DAS**, and **Sul-Nap**, able to detect Al(III) based on fluorescence in living cells. In the future, we will further optimize the structures of the molecules in order to improve their metal specificity and cytotoxicity.

3.4. Experimental Sections

3.4.1. Imaging Experiments in Living Cells

HeLa cells (ATCC, Manassas, USA) were maintained in media containing Dulbecco modified eagle medium (DMEM), 10% fetal bovine serum (FBS, GIBCO, Grand Island, NY, USA), 100 U/mL penicillin (GIBCO), and 100 mg/mL streptomycin (GIBCO). The cells were grown in a humidified atmosphere with 5% CO_2 at 37 °C. Cells were seeded onto 6 well plate (SPL Life Sciences Co., Ltd., South Korea) at a density of 150,000 cells per 1 mL and then incubated at 37 °C for 16 h. For imaging experiments, cells were first treated with compound [dissolved in DMSO; 1% v/v final DMSO concentration; 5 μM (for **TP-DAS**) or 20 μM (for **AIC-Jul** and **Sul-Nap**); at room temperature]. After 10 min, aluminum nitrate (dissolved in water; 1% v/v final concentration; 0-300 μM) is introduced to cells for 10 min. In case of fluorescence quenching experiments for **AIC-Jul**, cells were first treated with the compound (dissolved in DMSO; 1 % v/v final DMSO concentration; 20 μM; at room temperature). After 5 min, aluminum nitrite (dissolved in water; 200 μM; 1% v/v) was incubated with cells 10 min. Various concentrations of PPi (dissolved in bis-tris buffer; 1% v/v) were introduced to cells for 5 min and the cells were washed with 3 mL of bis-tris buffer three times. Imaging experiments were performed with an EVOS FL fluorescence microscope (Life Technologies) using a

ULSAN NATIONAL INSTITUTE OF SCIENCE AND TECHNOLOGY

DAPI light cube [for **TP-DAS**; excitation 357 (± 22) nm; emission 447 (± 30) nm] or GFP light cube [for **AIC-Jul** and **Sul-Nap**; excitation 470 (± 11) nm; emission 510 (± 21) nm].

3.5. Acknowledgements

This work was supported by the National Research Foundation of Korea (NRF) Grant funded by the Korean Government [NRF-2014R1A2A2A01004877 and NRF-2014S1A2A2028270 to M.H.L.]

3.6. References

1. Tomljenovic, L. *J. Alzheimers Dis*. **2011**, *23*, 567–598.
2. Walton, J. R. *Neurotoxicology* **2009**, *30*, 1059–1069.
3. Siegel, N.; Haug, A. *Biochim. Biophys. Acta* **1983**, *744*, 36–45.
4. Roskams, A. J.; Connor, J. R. *Proc. Natl. Acad. Sci. U. S. A.* **1990**, *87*, 9024–9027.
5. Kepp, K. P. *Chem. Rev.* **2012**, *112*, 5193–5239.
6. Chen, W.-T.; Lia, Y.-H.; Yu, H.-M.; Cheng, I. H.; Chen, Y.-R. *J. Biol. Chem.* **2011**, *285*, 9646–9656.
7. Jing, Y.; Wang, Z.; Song, Y. *Synapse* **2004**, *52*, 292–298.
8. Candy, J. M.; Oakley, A. E.; Mountfort, S. A.; Taylor, G. A.; Morris, C. M.; Bishop, H. E.; Edwardson, J. A. *Biol. Cell* **1992**, *74*, 109–118.
9. Jo, T. G.; Bok, K. H.; Han, J.; Lim, M. H.; Kim, C. *Dyes Pigm.* **2017**, *139*, 136–147.
10. Jeong, H. Y.; Lee, S. Y.; Han, J.; Lim, M. H.; Kim, C. *Tetrahedron* **2017**, *73*, 2690–2697.
11. Jo, T. G.; Jung, J. M.; Han, J.; Lim, M. H.; Kim, C. *RSC Adv.* **2017**, *7*, 28723–28732.

ULSAN NATIONAL INSTITUTE OF
SCIENCE AND TECHNOLOGY

Acknowledgement

I appreciate all the people who have contributed to the completion of the work described in this thesis.

First and foremost, I would love to express my sincere gratitude to my advisor, Professor Mi Hee Lim for guidance and encouragement that she has provided during my M.S. course. She has continuously given me a great confidence to make a progress in research. Despite her busy schedules, she readily spent her valuable time for supervision, discussion, and inspiration regarding my project. Her advice was always helpful for me to establish the research goals and move forward as an independent researcher. Without her notable mentorship, motivation, and immense knowledge, I would not be able to accomplish my M.S. degree.

Additionally, I thank my committee members, Professors Tae-Hyuk Kwon and Jung-Min Kee, for investing their precious time for providing insightful advice.

I want to also acknowledge my collaborators who have continuously helped me carry out the works described in this thesis. Particularly, I would like to express appreciation to Professor Junghyun Chae, Kyu Yeon Kim, Dr. Shin Jung Lee, and Professor Jaeheung Cho for cooperation regarding the preparation of small molecules and discussion regarding experimental results.

Importantly, thank all of the Lim Lab group members, Dr. Hyuck Jin Lee, Juhye Kang, Geewoo Nam, Eunju Nam, Yonghwan Ji, Misun Lee, Mingeun Kim, Nahye Park, Jong-Min Suh, Yelim Yi, Gunhee Kim, and Juri Lee, and our previous group members (Michael W. Beck and Jeffrey S. Derrick) for their assistance and lively scientific discussion. In addition, I thank our lab manager, Mi Sook Lim, for her administration and support for our laboratory. I was considerably inspired by their consideration, knowledge, sincerity, and diligence. It was a great honor for me to work with our group members at UNIST.

Lastly, I would love to appreciate my parents, Woong Ku Han and Jeong Ha Kim, and my brother, Seok Woo Han, with their strong support and encouragement that have allowed me to focus on achieving my research goals during my M.S. course.

Jiyeon Han

Department of Chemistry
Ulsan National Institute of Science and Technology (UNIST)
UNIST-gil 50, Ulsan 44919, Republic of Korea
Office Phone: +82-52-217-5456
Email: jiyeonhan@unist.ac.kr

Education

Mar. 2012 – Aug. 2016 **B.S., Chemistry, Ulsan National Institute of Science and Technology (UNIST), Ulsan, Korea**
Graduated *Summa Cum Laude*

Sep. 2016 – Feb. 2017 **M.S., Chemistry, Ulsan National Institute of Science and Technology (UNIST), Ulsan, Korea**
Advisor: Professor Mi Hee Lim
Thesis Title:
Development of Novel Chemical Tools towards Single or Multiple Pathogenic Elements in Alzheimer's Disease

Honors, Awards, and Scholarships

July 2017 **Poster Award**
The 2017 Bioinorganic Chemistry Symposium, Suanbo, Korea

Feb. 2017 **Ulsan City Mayor's Award**
Ulsan, Korea

Sep. 2016 – Present **Research or Teaching Assistant (TA) Scholarships**
Ulsan National Institute of Science and Technology (UNIST), Ulsan, Korea

Sep. 2015 – Feb. 2016 **National Scholarship for Science and Engineering**
Korea Student Aid Foundation, Seoul, Korea

Mar. 2012 – Aug. 2016 **Full Scholarship**
Ulsan National Institute of Science and Technology (UNIST), Ulsan, Korea

Publications

10. Min Seon Kim, Tae Geun Jo, **Jiyeon Han**, Mi Hee Lim, and Cheal Kim* *Submitted for Publication*, **2018**.
"A Fluorescent and Colorimetric Schiff Base Chemosensor for the Detection of Zn^{2+} and Cu^{2+}: Application in Living Cell Imaging and Colorimetric Test Kit"

9. Ji Hye Kang, **Jiyeon Han**, Mi Hee Lim, and Cheal Kim* *Submitted for Publication*, **2018**.
"An Aminohydantoin-based Fluorescent Chemosensor for the Sequential Detection of Zn^{2+} and Pyrophosphate in Aqueous Media and Living Cells"

8. Jae Min Jung, Ji Hye Kang, **Jiyeon Han**, Hyojin Lee, Mi Hee Lim, Ki-Tae Kim, and Cheal Kim* *Submitted for Publication*, **2018**.
"Sequential Detection of Zn^{2+} and Sulfide by an "Off-on-off" Type Fluorescent Chemosensor in Living Cells and Zebrafish Larvae"

7. **Jiyeon Han**, Hyuck Jin Lee, Kyu Yeon Kim, Shin Jung C. Lee, Jong-Min Suh, Jaeheung Cho, Junghyun Chae,* and Mi Hee Lim* *ACS Chem. Neurosci.* **2018**, *In Press*.
"Tuning Structures and Properties for Developing Novel Chemical Tools towards Distinct Pathogenic Elements in Alzheimer's Disease"

6. Jin Yeong Yun, Tae Geun Jo, **Jiyeon Han**, Hyu Jung Jang, Mi Hee Lim, and Cheal Kim* *Sens. Actuators B Chem.* **2018**, *255*, 3108–3116.
"A Highly Sensitive and Selective Fluorescent Chemosensor for the Sequential Recognition of Zn^{2+} and S^{2-} in Living Cells and Aqueous Media"

5. Eunju Nam,† **Jiyeon Han**,† Jong-Min Suh, Yelim Yi, and Mi Hee Lim* *Curr. Opin. Chem.Biol.* **2018**, *43*, 8–14. (†co-first authorship)
"Link of Impaired Metal Ion Homeostasis to Mitochondrial Dysfunction in Neurons"

4. Tae Geun Jo, Jae Min Jung, **Jiyeon Han**, Mi Hee Lim, and Cheal Kim* *RSC Adv.* **2017**, *7*, 28723–28732.
"A Single Fluorescent Chemosensor for Multiple Targets Cu^{2+}, $Fe^{2+/3+}$ and Al^{3+} in Living Cells and a Near-Perfect Aqueous Solution"

3. Ha Yeong Jeong, Seong Yeol Lee,* **Jiyeon Han**, Mi Hee Lim,* and Cheal Kim* *Tetrahedron* **2017**, *73*, 2690–2697.
"Thiophene and Diethylaminophenol-based "Turn-on" Fluorescence Chemosensor for Detection of Al^{3+} and F^{-} in a Near-Perfect Aqueous Solution"

2. Tae Geun Jo, Kwon Hee Bok, **Jiyeon Han**, Mi Hee Lim, and Cheal Kim* *Dyes Pigm.* **2017**, *139*, 136–147.
"Colorimetric Detection of Fe^{3+} and Fe^{2+} and Sequential Fluorescent Detection of Al^{3+} and Pyrophosphate by an Imidazole-based Chemosensor in a Near-Perfect Aqueous Solution"

1. Michael W. Beck, Jeffrey S. Derrick, Richard A. Kerr, Shin Bi Oh, Woo Jong Cho, Shin Jung C. Lee, Yonghwan Ji, **Jiyeon Han**, Zahra Aliakbar Tehrani, Nayoung Suh, Sujeong Kim, Scott D. Larsen, Kwang S. Kim,* Joo-Yong Lee,* Brandon T. Ruotolo,* and Mi Hee Lim* *Nat. Commun*. **2016**, *7*, 13115.
"Structure-Mechanism-Based Engineering of Chemical Regulators for Distinct Pathological Factors in Alzheimer's Disease "

Presentations

4. ***Oral Presentation***, The 120th General Meeting of the Korean Chemical Society, SRC Symposium, Biomimetic Catalysis Based on Porous Platform (BCP^2), Gwangju, Korea, October 18, 2017
Jiyeon Han, Hyuck Jin Lee, Jaeheung Cho, Junghyun Chae,* and Mi Hee Lim*
"Novel Chemical Regulators for Distinct Redox-active Pathogenic Elements in Alzheimer's Disease"

3. **Poster**, The 120th General Meeting of the Korean Chemical Society, Gwangju, Korea, October 18-20, 2017
Jiyeon Han, Hyuck Jin Lee, Jaeheung Cho, Junghyun Chae,* and Mi Hee Lim*
"Redox-tuning of Small Molecules to Develop Chemical Regulators for Multiple Pathogenic Elements in Alzheimer's Disease"

2. **Poster**, The 2017 Bioinorganic Chemistry Symposium, Suanbo, Korea, July 19-20, 2017
Jiyeon Han, Hyuck Jin Lee, Kyu Yeon Kim, Shin Jung C. Lee, Jaeheung Cho, Junghyun Chae,* and Mi Hee Lim*
"Chemical Regulators Containing Two Redox-Active Structural Moieties against Multiple Pathogenic Features in Alzheimer's Disease"

1. **Poster**, The 2016 Bioinorganic Chemistry Symposium, Suanbo, Korea, July 18-19, 2017
Jiyeon Han, Hyuck Jin Lee, and Mi Hee Lim*
"Tuning the Ability of a Small Molecule to Modulate Metal-Associated Amyloid-β Aggregation in Alzheimer's Disease"